UNITED NATIONS EDUCATIONAL, SCIENTIFIC AND CULTURAL ORGANIZATION
INTERNATIONAL ATOMIC ENERGY AGENCY
INTERNATIONAL CENTRE FOR THEORETICAL PHYSICS
I.C.T.P., P.O. BOX 586, 34100 TRIESTE, ITALY, CABLE: CENTRATOM TRIESTE

SMR/1006 - 11

COURSE ON "OCEAN-ATMOSPHERE INTERACTIONS IN THE TROPICS"
26 May - 6 June 1997

"On the Structure and Evolution of ENSO-Related Climate Variability in the Tropical Pacific: Lessons from TOGA"

presented by

D. BATTISTI
Dept of Atmospheric Sciences
University of Washington
Seattle WA
USA

Please note: These are preliminary notes intended for internal distribution only.

On the structure and evolution of ENSO-related climate variability in the tropical Pacific: lessons from TOGA

John M. Wallace[1], Eugene M. Rasmusson[2], Todd P. Mitchell[1],
Vernon E. Kousky[3], Edward S. Sarachik[1], and Hans von Storch[4]

[1] Joint Institute for the Study of the Atmosphere and Ocean, University of Washington, Seattle, Washington, U.S.A.

[2] Department of Meteorology, University of Maryland, College Park, Maryland, U.S.A.

[3] NOAA / NCEP Climate Prediction Center, Washington, D.C., U.S.A.

[4] Institute of Hydrophysics, GKSS, Geesthacht, Germany

Short title: Observed Tropical Pacific ENSO Variability

Journal of Geophysical Research, Oceans

Submitted 20 June 1996

Revision as of 3 March 1997

PostScript files are available on http://tao.atmos.washington.edu/rasmusson

JISAO contribution 376

Abstract

Improved observations in the tropical Pacific during the TOGA program have served to corroborate preexisting notions concerning the seasonally dependent relationships between sea surface temperature, wind stress, rainfall, upper tropospheric circulation, and ocean thermal structure anomalies in the El Niño / Southern Oscillation (ENSO) phenomenon. However, the paradigm of a quasi-periodic "ENSO cycle", phased locked with the annual march, does not capture the complexity of the evolution of the anomalies. The inadequacy of this model was particularly apparent during the second half of TOGA when the variability was highly aperiodic. Nor does a single modal structure or empirical orthogonal function appear to be capable of representing the range of spatial patterns of ocean-atmosphere interaction in the tropical Pacific. These results suggest the need for a more inclusive phenomenological description of ENSO.

TOGA data serve to confirm the influence of tropical Atlantic SST anomalies upon rainfall in Northeast Brazil.

1. Introduction

A distinguishing characteristic of the TOGA Program was its strong phenomenological focus. It was inspired and molded by the scientific community's perceptions that (1) the El Niño / Southern Oscillation phenomenon (ENSO) is the primary source of global interannual climate variability, (2) ENSO owes its existence to coupled ocean-atmosphere interactions in the tropical Pacific, and (3) the coupled system exhibits a degree of predictability on the seasonal time scale. This article begins with a review of the observations, the scientific investigations, and the climate events that gave rise to these perceptions, with emphasis on phenomena in the tropical Pacific. This historical background is followed in section 3 by a documentation of the ENSO-related variability in the tropical Pacific during the TOGA decade. Section 4 surveys large scale, coupled ocean-atmosphere interaction in the tropical Atlantic and Indian Oceans. The final section reflects upon how the observations taken during the TOGA decade have modified preexisting notions concerning the structure and evolution of the ENSO phenomenon in particular and coupled tropical ocean-global atmosphere variability in general.

2. Historical Background

The recognition of ENSO as a coupled ocean-atmosphere phenomenon and the appreciation of its important role in seasonal-to-interannual climate variability were not the result of a single dramatic scientific "breakthrough"; rather they developed out of a series of studies spanning a period of more than six decades.

2.1 Early Investigations

The first significant step down the path to the recognition and understanding of ENSO was a study by *Brooks and Braby* [1921], who noticed that long lasting wet and dry regimes at island stations in the western and central equatorial Pacific tend to be spatially coherent across a broad longitude belt, and associated with interannual variations in the surface wind field. It is now clear

that this relationship between the equatorial easterlies and equatorial Pacific rainfall is a fundamental feature of ENSO variability.

Three years later, *Walker* [1924] published the landmark synthesis of his studies of coherent global variability in which he described the broad scale characteristics of the Southern Oscillation in terms of the sea level pressure (SLP), surface temperature and rainfall variability. The linkage between the Southern Oscillation (SO) and the equatorial Pacific variations discovered by Brooks and Braby was forged a decade later in a paper entitled "Marquesan Meteorology" by *Leighly* [1933] that was truly remarkable for its time. It included a discussion of the relationship between year-to-year rainfall variations in the Marquesas Islands (centered near 10°S, 140°W) and climate anomalies in the equatorial trough zone (i.e., the belt of low SLP separating the subtropical anticyclones of the Northern and Southern Hemispheres). Leighly deduced the fundamental relationship between sea surface temperature (SST) gradient, surface wind, and rainfall from simple two-station SLP differences, long before Darwin. Australia (12°S, 131°E) and Tahiti (17°S, 150°W) data began to be used routinely to monitor the SO. The fact that Leighly did not have access to SST data makes his deductions all the more impressive. His insight is well illustrated by the following quotation: "if, as may reasonably be concluded, the temperature of the ocean surface varies inversely with the force of the east winds of the equatorial belt, periods of steep (surface pressure) gradient westward should also be periods of low water temperature, and thus unfavorable to rain on the mid-Pacific islands. This consideration supplies an explanation of the association of low temperature and drought, and conversely of high temperature and abundant rain. In the absence of further observational data on oceanic temperature, relative importance cannot be assigned to atmospheric circulation and water surface temperature as factors in the determination of rainfall fluctuations in the Marquesas. Since the two factors operate in conjunction, and result from the same fundamental causes, their effects would be difficult to separate". Unfortunately, the lack of citations of this remarkable paper indicates that it had little or no impact on the sequence of studies culminating with the paper in which *Bjerknes* [1969] firmly established the Pacific

relationship between Walker's SO and SST variations in the tropical Pacific. It appears that the first citation of Leighly's paper did not occur until *Julian and Chervin* [1978] recognized its significance in the context of their review of the SO and Walker Circulation phenomenon.

Following upon several decades of relatively weak and irregular behavior, ENSO-related climate variability became stronger and more cyclic in the 1950's . The major warming of 1957–58 provided data for a study by *Ichiye and Peterson* [1963] in which they hypothesized, for the first time, that ocean-atmosphere interaction is central to the evolution of the wind, SST and rainfall fields in the equatorial Pacific. *Berlage* [1966] examined the dominant time scales of the SO, and identified a link between the SO and the episodic warmings of SST along the coast of southern Ecuador and northern Peru known locally as El Niño [*Eguiguren,* 1894; *Murphy,* 1926; *Lobell,* 1942]. Subsequently, *Doberitz* [1968] used cross-spectrum analysis to quantify relationships between SST, surface wind, and rainfall in the equatorial dry zone of the central and eastern equatorial Pacific.

2.2 Bjerknes' Synthesis

Television pictures from weather satellites, launched during the 1960's, provided new insight into the climatological-mean cloud and rainfall fields over the equatorial Pacific, and their evolution during the continuing sequence of large amplitude swings of the SO and the related El Niño phenomenon. This improved definition of the rainfall patterns set the stage for a seminal ENSO synthesis by *Bjerknes* [1969]. Integrating the new information from satellites with conventional surface and upper air observations from Canton Island in the context of earlier studies dating back to those of Gilbert Walker, Bjerknes identified coupled ocean-atmosphere interactions in the equatorial Pacific as the source of ENSO-related climate variability. In his comprehensive description of these interactions, the central climatic feature is the east-west SST gradient between the pronounced dry zone over the cold waters of the eastern equatorial Pacific and the heavy convective rainfall over the warm waters of the western equatorial Pacific. Bjerknes viewed the

equatorial easterlies that link these areas of sinking and rising air as the lower branch of an east-west equatorial "Walker Circulation", driven by the basin-scale SST gradient. He proposed that variations in the Walker circulation couple the circulation field of Walker's SO to the zonal gradient of SST in the equatorial Pacific. While the regional El Niño phenomenon of the eastern equatorial Pacific remains part of the picture in his explanation, the central feature is the basin-scale oscillation in SST that forces the planetary-scale circulation anomalies associated with the SO.

Bjerknes [1969] characterized the feedback process between ocean and atmosphere as follows: "A change toward a steeper pressure slope at the base of the Walker Circulation is associated with an increase in the equatorial easterly winds and hence also with an increase in the upwelling and a sharpening of the contrast of surface temperature between the eastern and western equatorial Pacific. This chain reaction shows that an intensifying Walker Circulation also provides for an increase of the east-west temperature contrast that is the cause of the Walker Circulation in the first place. On the other hand, a case can also be made for a trend of decreasing speed of the Walker Circulation ...." .

While the notion of a positive feedback between SST and atmospheric circulation seemed well supported by the evidence, the fundamental question of how the coupled system evolves from the warm state to the cold state and vice versa remained to be answered. In the words of *Bjerknes* [1969]: "There is thus ample reason for a never-ending succession of alternating trends by air-sea interaction in the equatorial belt, but just how the turnabouts between trends takes place is not quite clear." Answering this question required overcoming two major obstacles. The first was the primitive understanding of equatorial ocean dynamics that existed at that time, and this contributed to the second, the lack of a coupled modeling capability. With only a few exceptions, e.g. *McWilliams and Gent* [1978], theoretical and modeling studies prior to TOGA primarily focused on the two simpler "uncoupled" questions, (1) "What is the equatorial Pacific ocean response to anomalous wind forcing?", and (2) "What is the global atmospheric response to equatorial Pacific SST anomalies?" The question of why the coupled system oscillates remained for TOGA to address.

2.3 The Canonical El Niño

Bjerknes' synthesis stimulated numerous observational studies, which, by the early 1980's, provided a much improved description of the structure and evolution of ENSO. Some of these studies contributed to a better description of its structure and spatial extent: e.g. *Trenberth* [1976], *Weare et al.* [1976], *Quinn et al.* [1978], *van Loon and Madden* [1981], and *Pazan and Meyers* [1982]. Others were more focused on the evolution of the tropical Pacific warm phase anomaly fields, e.g., *Wooster and Guillen* [1974], *Ramage and Hori* [1981], and *Weare* [1982]. A description of the typical evolution of the warm phase anomaly fields emerged from these studies, which was referred to by *Cane* [1983] as the "canonical El Niño". Particularly influential in this development were the papers of *Wyrtki* [1975], and *Rasmusson and Carpenter* [1982].

On the basis of a study of the evolution of the equatorial wind and sea level fields during the 1957–58, 1965, and 1972–73 warm episodes, *Wyrtki* [1975] concluded that El Niño warmings along the South American coast are not the result of local changes in surface wind forcing (i.e. decreased upwelling), as previously thought, but rather reflect a remote SST response to a rapid decrease in the easterlies in the equatorial central Pacific. He described a sequence of events culminating in the onset of a coastal warming. It begins with a "buildup phase" of abnormally strong equatorial easterlies, during which the slope of the sea level and the thermocline across the equatorial Pacific increases, as warm water accumulates on the western side of the basin. The termination of this regime is marked by a rapid collapse of the easterlies, which remained unexplained, since Wyrtki was not addressing the coupled problem. The rapid decrease in the easterly wind stress excites an equatorial Kelvin wave, characterized by an eastward surge of warm surface water. With the arrival of the Kelvin wave in the eastern Pacific, the thermocline is depressed, and rapid warming ensues. Later studies [e.g., *Barber and Chavez*, 1983; *McPhaden and Picaut*, 1990] showed that the intensity of the upwelling during the warming is little changed, but the upwelled water is warmer, since it now originates from above rather than

below the deeper thermocline.

Wyrtki's scenario addressed the question of the onset of the coastal El Niño warming from the standpoint of the forcing of the ocean by an abrupt change in zonal wind stress, rather than the more slowly evolving basin-scale warming of the coupled system envisioned by *Bjerknes* [1969]. His study had significant implications for prediction of the coastal warming: i.e., that it would follow a precursor "buildup phase" and there would be a roughly two-month lag between the collapse of the easterlies and the arrival of the Kelvin wave at the coast. Simple ocean model simulations [*Hurlburt et al.*, 1976; *McCreary*, 1976; *Busalacchi and O'Brien*, 1981] and a subsequent analysis of the 1976 warming [*Wyrtki*, 1979] provided further evidence in support of this scenario.

Since the coastal El Niño warmings are associated, even in the Spanish name, with a particular season, there is reason to believe that the general pattern of ENSO-related anomalies may be constrained by the evolving annual march. With this in mind, *Rasmusson and Carpenter* [1982, hereafter RC] described the mean seasonal pattern of the warm episode wind, SST and rainfall anomaly fields in terms of seasonal composites, based on six major warm episodes that occurred between 1950 and 1976.

The warm episode composites suggested a fairly systematic evolution, which had the implication that the evolving pattern might be predictable once the episode is underway. In agreement with Wyrtki's study, the RC composite warm episodes showed stronger than normal equatorial easterlies to the west of the date line during the months preceding the onset of the warm episode. The easterly anomalies were replaced by westerly anomalies in the western Pacific during October-November of the year prior to the warming, accompanied by the appearance of positive equatorial SST anomalies near the date line. Larger positive SST anomalies developed in the eastern equatorial Pacific early in the following year, reaching maximum values around April-June. Positive SST anomalies expanded westward from the coast into the central equatorial Pacific in subsequent months, and the westerly wind anomalies in the central equatorial Pacific intensified,

becoming most strongly developed during August-December. During the following northern winter (December-February), which RC referred to as the "mature phase" of the warming, the positive SST and rainfall anomalies were concentrated in the central equatorial Pacific and the lower branch of the equatorially symmetric "Hadley circulation" was intensified in this sector, contributing to increased low-level convergence in the equatorial belt. The mature phase was followed, a season later, by a decay in the anomaly patterns, and their replacement by a developing pattern of cold phase anomalies. *Barnett's* [1983] analysis of maritime surface observations over the Pacific and Indian Oceans, based on complex empirical orthogonal function analysis, confirmed the sequence of evolution described above.

By 1982, the canonical El Niño was widely accepted as a reliable description of the sequence of events associated with a warm episode of what is sometimes termed the "ENSO cycle". Confidence in this conceptual model engendered an air of optimism regarding the prediction of the onset and evolution, if not the amplitude of warm episodes. This optimism was rudely dashed by the 1982–83 warm episode.

2.4 Lessons from the 1982–83 Warm Episode

The strong reliance on the canonical precursors and a subsequent evolution that is phase-locked to the annual march resulted in a significant delay in recognizing the 1982–83 episode for what it was. The observations available at that time, i.e., SLP data were adequate to define the status of the SO, and SST, sea-level height, surface and upper air wind analyses, and fields of outgoing longwave radiation (OLR: an indicator of deep convective cloudiness) were adequate to define the large-scale features of the developing anomaly fields. By August 1982, many of the characteristic features of warm episodes of the ENSO cycle were already in evidence. However, for lack of a significant "buildup phase" and because the warming propagated eastward across the basin from the central Pacific, rather than westward from the South American coast, the research community was caught off-guard. In retrospect, it seems clear that the delay in recognizing the developing 1982–83 warm episode was primarily due to a flawed conceptual framework rather than to the

inadequacy of the observations.

The marked departure of the 1982–83 warm episode from the RC canonical evolution based on analysis of the six prior major warm episodes raised a number of new questions. The post-mortem modeling and diagnostic studies that followed set the stage for the TOGA Program. The magnitude of the 1982–83 warm episode was of historical proportions, but how atypical was its evolution? Regarding the lack of a precursor "buildup phase," an extended period of above normal equatorial easterlies corresponds to a high index state of the SO, which is identified with the cold phase of the ENSO cycle. Examination of more extended time series of indices of the SO and equatorial Pacific SST indicates that not all significant warm episodes have been preceded by pronounced cold phases: e.g., *Rasmusson and Wallace* [1983] noted that the evolution of the 1940–41 warm episode, which predated the episodes used in the RC composite, was similar in many respects to the 1982–83 episode. Although the evolution of the 1982–83 warm episode did not conform to the RC composite, the seasonality of the Peru coast anomaly time series was generally similar. For example, the largest SST anomalies along the coast occurred early in the calendar year, as in prior events, but in contrast to the composite, this El Niño event occurred toward the end, rather than at the onset of the basin-wide warm episode.

On the eve of the TOGA Program, the canonical picture was being re-evaluated, and there was an increased diagnostic emphasis on the variations in the western Pacific warm pool. A new set of questions was emerging which included the event-to-event consistency and secular variability of the ENSO phenomenon.

3. ENSO Variability During TOGA

Fortunately for those who conceived, planned and implemented TOGA, the ENSO phenomenon exhibited a variety of behavior during the ten year lifetime of the program 1985–94, as evidenced by the extended time series of the SST "cold tongue index" shown in Fig. 1. The record breaking 1982–83 warm episode was followed by another well defined warm episode that

set in around August 1986 and lasted into early 1988 and a more prolonged warm period that spanned much of the early 1990's and exhibited several minor peaks. By some measures, the interval extending from April 1988 to mid 1989 was as cold in the equatorial Pacific as any period of comparable length since the mid 1950's. Compared to the the previous 35 years, the ENSO cycle from the late 1970's onward (including the TOGA decade) exhibited less of a tendency for phase locking with the annual cycle (with peaks coinciding with the "cold season" July-November indicated by the blue shaded bands in Fig. 1), and less of a tendency for a quasi-biennial rhythm [*Barnett*, 1983; *Rasmusson et al.*, 1990] than is apparent in segments of the 1950–76 record. *Trenberth and Shea* [1987] noted an analogous lack of stationarity with respect to the regularity of the ENSO cycle in earlier segments of the record.

Descriptions based on a single index do not do justice to the complexity of the climate variability over the equatorial Pacific during the TOGA decade. Figure 2 shows time series of the three SST indices defined by RC, together with the conventional Southern Oscillation Index (SOI). Niño 1+2 represents conditions off the Peru coast; Niño 3 an equatorial strip extending from 90° to 150°W; and Niño 4 an equatorial strip centered on the date line. The SOI is the normalized difference between normalized SLP differences: Tahiti minus Darwin. The major warm and cold episodes of the ENSO cycle are evident in all four series, but the correspondence between the amplitude and the timing of individual episodes is far from perfect. For example, the 1982–83 warm episode was much more prominent and persisted longer in Niño 1+2, than in Niño 4. The contrasts in the behavior of the indices are particularly notable during the second half of the TOGA decade (1990-94), when Niño 1+2 averaged only slightly above normal and exhibited a sequence of short lived warm and cold episodes, while Niño 4 exhibited what appeared to be a single, virtually uninterrupted warm episode, most of which is mirrored in the SOI.

In the following subsections we will consider separately the year-to-year variability of the ENSO cycle during the TOGA decade and the variations in the mean state of the tropical Pacific from the first to the second half of the TOGA decade.

3.1 Interannual Variability

The variability of SST within the equatorial Pacific waveguide (4°S–4°N) during the TOGA decade is displayed in a time versus longitude format in the middle panel of Fig. 3. The first five year period (1985–89) was dominated by swings from cold to warm and back to cold again in association with the onset and cessation of the 1986–87 warm episode and the 1988–89 cold episode that immediately followed, both of which rank among the major features in the 142 year long historical record in Fig. 1.

Consistent with the RC composite, the warm episode along the South American coast in 1987 peaked early in the calendar year, about 6 months in advance of the strongest basin-wide SST anomalies (Figs. 2 and 3). However, in contrast to the prevailing interpretation of the "canonical El Niño" [e.g., *Cane* 1983], the SST anomalies did not spread westward from the South American coast to the interior of the basin. Rather, it seems that the basin wide anomalies developed *in situ* while the coastal anomalies weakened. The lack of time continuity between these features is consistent with the results of *Trenberth and Shea* [1987], *Deser and Wallace* [1987], *Wright et al.* [1988], and *Trenberth and Hoar* [1996], which indicate that the coastal SST perturbations documented by *Quinn et al.* [1978] in reference to El Niño and the basin-wide SST perturbations that *Bjerknes* [1969] linked to the major swings of the SO are only weakly coupled.

Higher frequency variability is clearly evident in Fig. 3, superimposed upon the major swings of the ENSO cycle. For example, the 1988–89 cold episode was marked by two distinct extrema, which are also evident in Fig. 2: the first in the eastern part of the basin around May 1988 and the second centered near the date line about 6 months later. Weaker changes of opposite polarity were observed at the western end of the basin.

Consistent with Fig. 2, the variability during the second half of the TOGA decade (1990–94) was somewhat different in character from that observed during the first half. Strong positive SST

anomalies in the vicinity of the date line prevailed throughout virtually the entire period, while farther to the east SST exhibited weak, irregular fluctuations with a characteristic period on the order of a year. There were times during the second half of TOGA when SST was well above normal near the date line but near or below normal along the South American coast. Relatively short lived warm episodes peaked in mid-1991, early 1992 and 1993, and late 1994, of which the 1992 episode was the most prominent. Like the 1986–87 warm episode, the 1992 and 1993 episodes were accompanied by negative SST anomalies at the western end of the basin and westerly equatorial wind stress anomalies (indicated by the vectors in Fig. 3).

The left hand panel of Fig. 3 shows the corresponding time-longitude section of the anomalies in the depth of the 20°C isotherm along the equator, an indicator of displacements in the thermocline depth, obtained from the data assimilation system of the NOAA / NCEP model. As documented in the companion paper of *McPhaden et al.* [1997], these displacements are largely a reflection of the response of the ocean model to variations in equatorial wind stress. In the eastern half of the basin they closely match the SST anomalies, even with respect to the minor features pointed out above. There also appears to be a rough correspondence between the SST and thermocline displacement anomalies at the western end of the basin. For reasons that are not clear to us, the major displacements exhibited a preference for eastward phase propagation during the TOGA decade, with individual features crossing the Pacific basin in about a year, whereas the SST anomalies exhibited no such preference. Conversely, the distinct suggestion of a nodal line along 160°E in the SST anomaly pattern is not evident in the thermocline displacement.

The major advances in satellite monitoring of tropical rainfall during the TOGA decade have revealed the full extent of the correspondence between rainfall and the strength of the tradewinds in the equatorial belt, first pointed out by *Brooks and Braby* [1921]. The distribution of equatorial (5°N–5°S) rainfall anomalies as inferred from microwave satellite imagery using the algorithm developed by *Spencer* [1993] is shown in the right hand panel of Fig. 3. As documented in the Appendix, the features in this analysis are generally consistent with rainfall estimates based on SSM/I imagery [*Ferraro et al.*, 1996], with *the* GOES Precipitation Index (GPI) based on high

resolution infrared satellite imagery [*Joyce and Arkin, 1996*], and with the rainfall estimates based on a blend of *in situ* and satellite measurements and numerical weather prediction model output [*Xie and Arkin,* 1996]. In general, the rainfall anomalies match the SST anomalies remarkably well, even with respect to the high frequency fluctuations. In agreement with many previous studies, the zonal structure of the two fields is somewhat different: the node in the rainfall anomaly pattern is about 15° to the west of the node in the SST anomaly pattern and the stronger rainfall anomalies tend to be somewhat more concentrated in the central Pacific (but not nearly as much so as in the corresponding OLR section shown in the left panel of Fig. A1).

Figure 4 is the counterpart of Fig. 3 for the total fields, including the seasonally varying climatological means. The annual march dominates the SST variability in the equatorial eastern Pacific. In contrast to the SST anomalies shown in the previous figure, the SST perturbations associated with the annual march really do propagate westward from the South American coast to the date line over a period of several months, as shown previously by *Wyrtki* [1965] and *Horel* [1982]. Near the coast, an El Niño event can be viewed as an enhancement of the climatological-mean warm season [*Wyrtki,* 1975], as manifested in the pink strips extending westward from the coast in the early months of 1987, 1992, and 1993. Farther to the west, where the annual march is rather weak and there exists a strong year-round east-to-west SST gradient, the zonal excursions of the isotherms resemble the Niño 4 temperature plot in Fig. 2: warm episodes correspond to an eastward expansion of the "warm pool", delineated by the 28 or 29 °C isotherm [*McPhaden and Picaut,* 1990; *Picaut et al.,* 1996].

East of the date line, the section for the rainfall, shown in the right panel of Fig. 4, exhibits a strong annual march with a distinct wet season that closely parallels the warm season in the SST section, including the westward propagation. Years with warmer than normal warm seasons tend to be characterized by strong and/or abnormally long rainy seasons. Farther to the west, the annual march is less pronounced. During warm episodes the zone of year-round heavy rainfall over the western Pacific expands eastward with the "warm pool", bringing with it an increase in rainfall,

even during the dry season.

The lower panel of Fig. 5 shows the zonally averaged SST anomalies in the tropical Pacific from the date line eastward in a time-latitude format, dating back to mid-1981. This mode of presentation distinguishes more clearly between the higher frequency fluctuations with periods on the order of a year, which tend to be largely restricted to the equatorial zone and the lower frequency variability, which tends to be relatively more prominent off the equator. The equatorial symmetry in this figure is quite striking. The characteristic bowed shape of many of the contours is indicative of tendency for SST perturbations on the equator to lead those off the equator, consistent with the notion that SST within ~10° of the equator is strongly influenced by the time varying volume and temperature of the water upwelled within 1° of the equator. The narrowness of the upwelling zone relative to the cold tongue is evident in the signature of the phytoplankton in high resolution coastal zone color scanner satellite imagery and in the mean meridional motions of drifting buoys [*Poulain*, 1993]. As in the time-longitude sections, warm episodes coincide with westerly wind anomalies along the equatorial western and central Pacific, and vice versa. The associated off-equatorial meridional wind anomalies characteristic of the "mature phase" of the RC composite are also clearly evident. The corresponding zonally averaged rainfall anomalies, shown in the upper panel of Fig. 5, exhibit a less clearly defined meridional structure, and some tendency for the largest anomalies to be biased toward the north of the equator, toward the climatological-mean intertropical convergence zone (ITCZ). These differences notwithstanding, the timing of the anomalies agrees quite well with those in the SST section.

Figure 6 is the counterpart of Fig. 5 for the total fields of rainfall and SST, including the seasonally varying climatological means. In the annual mean, the ITCZ in the rainfall pattern coincides with the warmest water along 10°N and the equatorial dry zone coincides with the cold tongue in the SST. A weak Southern Hemisphere ITCZ makes a brief appearance along 7°S in February-March of the warmer years: it is apparent in the MSU, SSM/I, and GPI rainfall climatologies, distinct from the South Pacific Convergence Zone farther to the west. Heavy

rainfall never intrudes into the equatorial dry zone during the cold season, but during the warm seasons of the stronger warm episodes the dry zone was virtually obliterated. The correspondence between the SST and rainfall distributions is quite striking: even the irregularities from one year to the next match quite well.

Figures 7 and 8 provide an overview of the global anomaly patterns associated with the ENSO cycle during the first nine years of the TOGA decade. They were constructed by regressing the global fields listed in the figure captions upon the time series of cold tongue SST in Fig. 1. The patterns and their amplitudes are representative of conditions observed during the warm phase of a weak swing of the ENSO cycle. Figure 7 is based entirely upon observed fields, while Fig. 8 contains model derived fields from the NCEP/NCAR Reanalysis Project [*Bengtsson and Shukla,* 1988; *Kalnay et al.*, 1996] that was set in motion during the TOGA period and is now nearing completion.

Observed SST and surface wind anomalies shown in the lower panel of Fig. 7 strongly resemble the patterns in the RC warm episode composite and the leading nonseasonal empirical orthogonal function (EOF) of Pacific SST of *Weare et al.* [1976], both of which are based on pre-TOGA data. The winds derived from the reanalysis (Fig. 8) capture the major features of the observed winds except for the patch of southerly anomalies in the equatorial eastern Pacific, which may be a shallow boundary layer feature, unrelated to the SLP field [*Wallace et al.*, 1989]. A distinctive SO signature reminiscent of Fig. 1 of *Trenberth and Shea* [1987] is evident in the SLP anomalies shown in the middle panels. (The resemblance is even stronger if correlation coefficients are plotted instead of regression coefficients.) The reanalyzed pressure field captures the spatially coherent structures inherent in the COADS data. The Microwave Sounding Unit (MSU) rainfall anomalies are not quite as well replicated in the reanalysis: instead of being broadly distributed throughout the outer part of the climatological-mean equatorial dry zone, they tend to be somewhat more concentrated along the equator near 160°W. The band of enhanced rainfall along the northern periphery of the dry zone in the satellite observations ties in well with the enhanced rainfall observed over the Galapagos Is. and along the coast of Ecuador and northern Peru during

El Niño, whereas the corresponding feature in the reanalysis intersects the coast farther north, near Panama. Despite these discrepancies, the agreement between the two rainfall patterns is quite impressive when viewed from a global perspective.

The corresponding pattern of tropospheric (1000-200 hPa layer-mean) temperature anomalies, shown in the upper panels is dominated by the same distinctive "dumbbell pattern" in the tropical eastern Pacific that is apparent in the results of *Yulaeva and Wallace* [1994] based on the partially overlapping period of record 1979-91, which includes the 1982-83 event. The wave pattern in the equatorial belt is reminiscent of theoretical solutions of *Matsuno* [1966], *Webster* [1972], and *Gill* [1980]. Other features of interest are the prevalence of positive anomalies throughout the entire tropics, and the enhanced baroclinity along 30°N and 30°S over much of the Pacific and the Americas. The reanalysis captures the pattern in the satellite data extremely well, except for the relative minimum in the equatorial western Pacific.

With the addition of the TOGA decade the period of record is now sufficiently long so that the data can be stratified by season and by warm / cold phase of the ENSO cycle. *Mitchell and Wallace* [1996] show that the rainfall anomalies associated with the warm phase of the ENSO cycle tend to be stronger and penetrate deeper into the core of the equatorial dry zone during the warm season December-May than during the cold season July-November. Presumably during the cold season SST in the interior of the dry zone remains below the 27°C threshold for deep convection [*Gadgil et al.*, 1984; *Graham and Barnett*, 1987], even during El Niño. *Hoerling et al.* [1997] show that for similar reasons, the SST and rainfall anomalies observed during the warm and cold phases of the ENSO cycle exhibit somewhat different spatial patterns. The warm phase is marked by a retreat of the cold tongue and the equatorial dry zone into the eastern Pacific, whereas the cold phase is characterized by a strengthening and westward expansion of the cold tongue and dry zone. Hence the anomaly patterns observed during the cold phase tend to be displaced westward relative to those observed during the warm phase, and *Hoerling et al.* demonstrate that this displacement has implications for the planetary-scale response.

3.2 Longer Term Variability

When viewed in the context of the entire 142-year time series in Fig. 1, a striking characteristic of the TOGA decade is the overall warmth of the second half (1990–94). Figure 9 shows the geographical distribution of the warming from 1985-89 to 1990-94, together with the corresponding changes in SLP, 850-hPa winds, and OLR. The changes are reminiscent of the differences in the respective fields between cold and warm episodes of the ENSO cycle on the interannual time scale, with pressure rises to the west of the date line and falls to the east, indicative of a drop in the SOI, a weakening of the easterlies along the equator, and an increase in rainfall in the equatorial central Pacific and farther to the east along the southern flank of the ITCZ. For further documentation of these changes the reader is referred to *Mantua and Graham* [1997].

Trenberth and Hoar [1996] noted that the prevalence of the warm polarity of the ENSO cycle throughout the second half of the TOGA decade is unprecedented in the 113 year record of a proxy SOI (Darwin SLP anomalies) that they examined and went on to speculate that this extraordinarily long warm episode might be indicative of a fundamental change in the character of the ENSO phenomenon, perhaps in response to the increase in global concentrations of greenhouse gases. The recurrence of the cold phase during 1995, which has persisted for over a year now (Fig. 2) makes this interpretation seem less plausible than it did a year ago. Furthermore, *Cane et al.* [1997] have argued that the signature of greenhouse warming should be characterized by enhanced upwelling in the equatorial Pacific, which would favor the cold, rather than the warm phase of the ENSO cycle.

The difference patterns in Fig. 9 are unprecedented in terms of their clarity (owing to the quality of the SST analyses during TOGA), but not in terms of their large scale structure: similar changes were observed for 5-year epochs 1977-82 minus 1971-76 [*Graham*, 1994]; for the decades 1977-86 minus 1967-76 [*Nitta and Yamada*, 1989]; and for the more extended epochs 1977-93 minus 1950-76 [*Zhang et al.*, 1997]. The SST pattern in Fig. 7 also resembles the

leading EOF's of lowpass filtered Pacific and global SST [*Wang*, 1995; *Yukimoto et al.*, 1997; *Zhang et al.*, 1997]. The pattern is clearly "ENSO-like" in many respects, but in comparison to the interannual variability associated with the ENSO cycle, the SST anomalies are less equatorially trapped, particularly in the eastern Pacific. This rather subtle distinction shows up more clearly in the EOF analyses cited above. The reasons for this apparent frequency dependence in the structure of the patterns are not well understood.

4. Coupled variations in the tropical Atlantic and Indian Ocean sectors

The standard deviation of SST in the tropical Atlantic and Indian Oceans is only about half as large as over the equatorial Pacific [*Hsiung and Newell*, 1983; *Bottomley et al.*, 1990], and the ratio is even smaller if only the spatially coherent portion of the variability, exclusive of the ENSO signal, is considered. Nevertheless, by the early 1980's it was already clear that coupled ocean-atmosphere variability over the tropical Atlantic sector is capable of impacting monsoon rainfall over the neighboring continents. In recognition of these promising results and in hopes that similar relationships might emerge in the Indian Ocean sector, the TOGA Program was defined as encompassing all three tropical oceans.

EOF analyses of SST anomalies in the tropical Atlantic by *Weare* [1977], *Lough* [1986], *Servain* [1991], and Zebiak [1993] revealed an array of spatially coherent patterns, including what appear to be an analogue of the ENSO variability in the Pacific. In contrast to the Pacific, where the ENSO variability dominates, off equatorial SST anomalies in the tropical Atlantic proved to be comparable in amplitude to those observed in the equatorial cold tongue. The off-equatorial anomalies have often been characterized in terms of a dipole mode, centered about the climatological-mean ITCZ. *Houghton and Tourre* [1992] have argued that they are more appropriately viewed as spatially coherent, but linearly independent modes of variability in the northern and southern tropics.

Hisard [1980], *Merle* [1980], and *Merle and Hisard* [1980] showed that SST and subsurface temperatures in the Atlantic cold tongue region in the Gulf of Guinea exhibit interannual variability analogous to the ENSO cycle in the eastern Pacific, and *Hisard* [1980] presented evidence that El Niño-like events are accompanied by anomalously heavy August rainfall along the Ivory Coast. As in the Pacific, the oceanic anomalies occur in response to a weakening of the easterlies in the western part of the basin [*Zebiak,* 1993]. *Horel et al.* [1986] and *Philander* [1986] have suggested that at least in some cases the wind anomalies should be viewed as a remote response to strong swings of the ENSO cycle in the Pacific. On the other hand, coupled modeling results of *Zebiak* [1993] suggest that they could arise from coupled ocean-atmosphere interactions analogous to, but distinct from those in the ENSO cycle. Results of *Carton and Huang* [1994] suggest that remote forcing from the Pacific is responsible for some of the warm events in the equatorial Atlantic, while local ocean-atmosphere interaction is responsible for others others. Studies of *Aceituno* [1988], *Curtis and Hastenrath* [1995], and *Nobre and Shukla* [1996] suggest that the remote forcing from the Pacific may also be responsible for some of the the off-equatorial SST anomalies in the tropical Atlantic.

The off-equatorial SST anomalies are strongly correlated with rainfall anomalies over Northeast Brazil [*Hastenrath and Heller* 1977; *Markham and McLain,* 1977; *Moura and Shukla,* 1981] indicative of shifts of the ITCZ in the western Atlantic from its seasonally varying climatological-mean position [*Hastenrath and Lamb,* 1977a,b; *Hastenrath and Greischar,* 1993]. They are accompanied by spatially coherent cross-equatorial surface wind anomalies [*Nobre and Shukla,* 1996] reminiscent of those observed in association with the climatological-mean annual march [*Mitchell and Wallace,* 1992]. Figure 10 shows the patterns of rainfall, SST, SLP and surface wind anomalies observed in association with positive rainfall anomalies over Northeast Brazil during the rainy season February-May, based on regression analysis, as described in the caption. Near the Brazil coast the nodes in the rainfall SST and SLP patterns and the axis of symmetry of the surface wind pattern coincide with the climatological-mean ITCZ. The polarities are dynamically consistent and indicative of a southward displacement of the ITCZ during the seasons

with above normal rainfall in Northeast Brazil. The SST anomalies are substantially weaker than those observed in the equatorial Pacific in association with ENSO, but the pattern is nonetheless quite robust, and there is ample evidence based on atmospheric general circulation model simulations that it is capable of forcing the observed rainfall anomalies [*Moura and Shukla*, 1981; *Mechoso et al.*, 1990]. The corresponding pattern for tropospheric layer averaged temperature (not shown) is much weaker and less distinct than its ENSO counterpart in Fig. 7.

Anomalies in monsoon rainfall in subsaharan West Africa have also been linked to SST anomalies in the tropical Atlantic [*Lamb*, 1978; *Folland et al.*, 1986; *Lough*, 1986; *Palmer*, 1986; *Parker et al.*, 1988; *Lamb and Peppler*, 1991; *Rowell et al.*, 1995]. Above normal rainfall in this region tends to be associated with negative SST anomalies in the Gulf of Guinea and positive SST anomalies in the western Atlantic poleward of 15°N. The observed correlations are not as strong as those involving Northeast Brazil rainfall, and their statistical significance is compromised by the marked decrease in rainfall over this region from the 1950's to the 1980's [*Nicholson*, 1993; *Rowell et al.*, 1995], which reduces the effective number of degrees of freedom inherent in the subsaharan rainfall time series relative to the Northeast Brazil series in Fig. 10. Nevertheless, the statistical relationships appear to be physically plausible and analogous to those for Northeast Brazil rainfall anomalies, and they have been replicated in atmospheric GCM (general circulation model) simulations with an early version of the United Kingdom Meteorological Office climate model [*Rowell et al.*, 1995].

The leading mode of SST variability in the tropical Indian Ocean is spatially amorphous and of the same polarity throughout the domain [*Weare*, 1979; *Navato et al.*, 1981]. Hence it is largely a reflection of variations in spatial-mean temperature, whose variability is highly correlated with ENSO indices [*Bottomley et al.*, 1990; *Yulaeva and Wallace*, 1994]. The fact that fluctuations in Indian Ocean SST are lagged by about a season relative to ENSO indices suggests that they occur in response to the ENSO cycle. This interpretation is supported by recent atmospheric GCM experiments by *Lau and Nath* [1994, 1996]. Spatial-mean SST over the tropical Indian Ocean is

strongly coupled with the interdecadal variability discussed in section 3.2 [*Nitta and Yamada,* 1989; *Kawamura*, 1994)].

Indian rainfall exhibits only a weak correlation with SST upstream over the Arabian Sea [*Shukla and Misra,* 1977; *Weare* 1979]. It is more strongly (positively) correlated with the SOI [*Walker, 1924; Pant and Parthasarathy,* 1981], and averages significantly below normal during monsoon seasons that fall within warm episodes of the ENSO cycle as defined by SST equatorial Pacific SST [*Rasmusson and Carpenter,* 1983]. Hence, in contrast to other tropical oceans, where SST and rainfall anomalies tend to be strongly coupled in a regional context, year-to-year variations in SST and rainfall over the Indian sector both appear to be remote responses to ENSO-related variability in the Pacific.

5. Lessons Learned from TOGA

The enhanced observations during the TOGA decade provided a clearer definition of the spatial patterns associated with the ENSO cycle than had hitherto been possible. The observed variability displayed many of the characteristics noted in the studies reviewed in Section 2. Basin-wide SST variations centered in the equatorial waveguide were tightly coupled to variations in zonal wind centered near the date line. Basin-wide warm episodes were accompanied by a weakening of the equatorial easterlies, by incursions of heavy rainfall into the equatorial dry zone, and by a local enhancement of the equatorially symmetric Hadley circulation in the Pacific sector. South American coastal warmings occurred in association with the basin-wide warm episodes, and they coincided with the climatological-mean warm season centered around February-April. In comparison to prior estimates based upon OLR, the new rainfall products available during TOGA tend to place greater emphasis upon the ITCZ and the associated rainfall anomalies to the east of the date line (Figs. A1 and A2). Instead of merely indicating an eastward shift of the belt of heavy rainfall over the western Pacific "warm pool" during warm episodes of the ENSO cycle, the new rainfall estimates indicate a major contraction and of the equatorial dry zone. The planetary-scale

atmospheric response to the rainfall anomalies exhibited the distinctive equatorially symmetric dipole pattern in tropospheric layer-mean temperature and 200-hPa streamfunction identified in previous studies.

There were aspects of the variability during the TOGA decade that did not conform to the "canonical El Niño" scenario. Like its predecessor in 1982–83, the 1986–88 basin-wide warm episode was not preceded by a coastal El Niño event. Yet despite the differences in sequencing, the seasonality inherent in the RC composite prevailed. Coastal El Niño events continued to be observed during the warm season and equatorial rainfall anomalies tended to be most pronounced in December through April, as documented in Fig. 3 and, in more detail in *Mitchell and Wallace* [1996]. A more fundamental departure from the RC scenario is the lack of coherence between the sequence of warm and cold episodes in different parts of the tropical Pacific. There were times during the early 1990's when it was difficult to define the status of the "ENSO cycle": e.g., some ENSO indices were indicative of the warm phase, while others were indicative of the cold phase.

The ambiguity in the status of the ENSO cycle during the second half of the TOGA decade is related to the broadening of the frequency spectrum of ENSO-related variability. The unifying rhythm that permeated SST time series throughout the tropical Pacific during the much of the 1960's and '70's was no longer in evidence. SST in the eastern equatorial Pacific exhibited high frequency fluctuations with periods as short as a year, while SST in the equatorial central Pacific and the off-equatorial eastern Pacific fluctuated with characteristic periods of a decade or longer. Aperiodic behavior is not unprecedented in the historical record: it was observed during the 1930's and 1940's [*Trenberth and Shea*, 1987]. Unfortunately the ENSO variability during that period has received relatively little attention because of concerns about the reliability of SST observations prior to the 1950's. It has not been until quite recently that the scientific community has had the opportunity to diagnose well documented ENSO-related variability in the absence of a dominant spatial pattern and rhythm.

Like the rhythms that characterize day-to-day weather fluctuations, the ENSO cycle fades in and out at irregular intervals. When it is strong, ENSO is likely to be more predictable [*Chen et*

al., 1995; *Davey et al.*, 1996; *Goddard and Graham*, 1997] and skillful forecasts are likely to be of more value, since it is the largest amplitude ENSO-related climate anomalies that produce the most significant societal impacts. Like society in general, operational climate prediction is subject to the vagaries of the ENSO cycle.

TOGA did not reveal the existence of any previously undiscovered SST / rainfall connections over the other tropical oceans. The most robust of these linkages still appears to be the one between February-May rainfall over Northeast Brazil and off-equatorial SST anomalies in the tropical Atlantic.

Acknowledgments. This work was supported by the NOAA Climate and Global Change Program through a grant to the Hayes Center. The authors wish to thank Ants Leetmaa, Mike McPhaden, Sumant Nigam, Jagadish Shukla, the reviewers Kevin Trenberth and David Karoly and the third anonymous reviewer, and the Editors Peter Webster and Lewis Rothstein for their contributions to this work.

Appendix: Satellite Rainfall Estimates

Figure A1 presents time-longitude sections of Pacific rainfall estimates from OLR [*Chelliah and Arkin*, 1992], GPI [*Joyce and Arkin*, 1996], SSM/I [*Ferraro et al.*, 1996], MSU, and a blend of rain gauge, GPI, two SSM/I products, and prediction model output [*Xie and Arkin*, 1996] for the period 1985–94. The meridional averages are taken for a band of latitudes centered slightly south of the equator to capture the largest ENSO-related east-west rainfall contrasts. The shading of OLR anomalies is chosen to be consistent with negative anomalies indicating greater than average rainfall. *Joyce and Arkin* [1996] present a similar comparison of GPI, MSU and SSM/I rainfall. Figure A2 documents the difference in OLR and MSU rainfall for December-January-February averages for 1986–87 minus 1988–89, seasons which are representative of the large swings in rainfall amounts between ENSO warm and cold episodes.

Figure Captions

Figure 1. Time series of monthly-mean SST anomalies (°C) averaged over the central and eastern equatorial Pacific (6°N–6°S, 180–90°W). Anomalies are with respect to the entire record. Successive nine- and five-point running mean filters have been applied to the time series. January–May (July–November) values are indicated by red (blue) shading. SST values for 1854–1992 obtained from the Comprehensive Ocean-Atmosphere Data Set (COADS) [*Woodruff et al.*, 1987, 1993] and for 1993–95 from NOAA / NCEP [*Reynolds and Smith*, 1994].

Figure 2. Time series of monthly-mean SST anomalies averaged over the Niño 1+2 (0–10°S, 90–80°W), Niño 3 (5°N–5°S, 150–90°W), and Niño 4 (5°N–5°S, 160°E–150°W) regions together with the conventional SOI (the normalized difference between normalized SLP: Tahiti minus Darwin) 1980 through April 1996. Each ordinate tick mark represents 1°C, or one standard deviation of the SOI time series. Anomalies in this and subsequent figures are with respect to the TOGA decade, 1985–94. Indices from the NOAA / NCEP Climate Prediction Center.

Figure 3. Longitude–time diagram of anomalies in equatorial Pacific 20°C isotherm depth (4.5°N–4.5°S), SST (4°N–4°S), and rainfall (5°N–5°S) for the TOGA decade. Arrows represent area-average zonal pseudo-stress over 4°N–4°S, 151°E–141°W. Positive (negative) values are indicated by red (blue) shading. Lightest (saturated) shading denotes isotherm depth, SST, and rainfall anomalies > 10m, 0.25°C, and 5 cm mon^{-1} (40m, 2°C, and 25 cm mon^{-1}) in magnitude, respectively. The largest magnitude zonal stress anomaly is -24 m^2 s^{-2}. Isotherm depths taken from the ocean data assimilation model at NOAA / NCEP; pseudo-stress from Florida State University [*Stricherz et al.*, 1992]; SST from NOAA / NCEP [*Reynolds and Smith*, 1994]; and Microwave Sounding Unit (MSU) rainfall from the NASA / Marshall Space Flight Center [*Spencer*, 1993]

Figure 4. As in Fig. 3, but for total fields. Progressively darker shading for 20°C isotherm depths > 60, 90, ..., 180 m; and rainfall amounts > 5, 20, 35, 50 cm mon^{-1}. SSTs < 26, 25, ... 22°C (>28, 29, 30°C) indicated by blue (red) shading with progressively greater saturation. The largest magnitude zonal pseudo-stress is –45 m^2 s^{-2}.

Figure 5. Latitude-time diagram of zonal-mean (180–90°W) anomalies in a) rainfall and b) SST and meridional pseudo-stress; and c) time series of equatorial (4°N–4°S) SST and zonal pseudo-stress anomalies averaged over 180–90°W and 151°E–141°W, respectively. Monthly-mean rainfall and SST means are centered at 1.25, 3.75, ..., and 1, 3, ... degrees latitude in each hemisphere, respectively. Positive and negative values shaded red and blue, respectively. Zonal-mean rainfall anomalies > 2.5 cm mon^{-1} in magnitude shaded with anomalies ranging from < –17 to > 22 cm mon^{-1}. Zonal-mean SST anomalies > 0.25 °C in magnitude shaded with values ranging from < –1.75 and > 1.25 °C. Seasonal-mean indices of coherent meridional pseudo-stress anomalies to the north and south of the equator (16–2°N, 151°E–141°W, and 6–20°S, 151°E–141°W, respectively) are plotted in vector format at their respective central latitudes (maximum vector magnitude plotted is 15 m^2 s^{-2}). Equatorial SST (°C) and zonal pseudo-stress anomalies (tens of m^2 s^{-2}) are depicted by shading and a contour in panel c, respectively. MSU rainfall, and pseudo-stress data sources as in Fig. 3; SST values from NOAA / NCEP for 1981 from *Smith et al.* [1996] and 1982–95 from *Reynolds and Smith* [1994].

Figure 6. As in Fig. 5, but for total fields. Zonal-mean rainfall shading interval of 2.5 cm mon^{-1} in magnitude shaded with values ranging from < 2.5 (blue) to 10 (white) to > 50 cm mon^{-1} (red). Zonal-mean SST shading interval of 0.5 °C with values ranging from < 23 (blue) to 27 (white) to > 29 °C (red).

Figure 7. Selected fields regressed upon monthly values of the cold tongue index time series shown in Fig. 1 for the period of record January 1985 through December 1993. All regressions are per one standard deviation of the reference time series. *Panel a):* tropospheric layer-mean temperature as deduced from Channel 2 of the MSU (contour interval 0.1 °C: negative contours are dashed) superimposed upon MSU rainfall (anomalies < -1, -2 cm mon^{-1} are shaded blue and > 1, 3, 5, and 7 cm mon^{-1} are shaded red, with more saturated colors for larger magnitude anomalies). *Panel b):* SLP (contour interval 0.25 mb: negative contours are dashed) superimposed upon rainfall as in the top panel. *Panel c):* Surface wind vectors superimposed upon SST. Only regression vectors > 0.5 m s^{-1} in magnitude are plotted; and the SST anomaly shading interval is 0.25 °C, with negative and positive anomalies shaded in blue and red, respectively. The SLP, surface vector wind, and SST were all obtained from the COADS. MSU source as in Fig. 3 and SLP, wind, and SST from the COADS. MSU channel 2 temperature estimates from *Spencer and Christy* [1990, 1992, 1993].

Figure 8. As in Fig. 7, but for similar fields from the NCEP reanalysis. *Panel a):* 1000-200 hPa layer-mean temperature superimposed upon rainfall. *Panel b):* SLP and surface vector wind superimposed upon rainfall. *Lower panel:* Surface vector wind superimposed upon SST (SST from *Reynolds and Smith* [1994]). Shading and contouring conventions as in Fig. 7.

Figure 9. Change from 1985–89 to 1990–94 in mean a) SST and 850 hPa vector wind, b) OLR and 850 hPa vector wind, and c) SLP and 850 hPa vector wind. Positive (negative) changes in scalar fields shaded red (blue), with no change indicated by a thick contour. SST, OLR, and SLP shading intervals of 0.2°C, 4 W m^{-2}, and 0.2 hPa, respectively. Reference vector wind difference magnitude is 5 m s^{-1}. SST source as in Fig. 3; 850–hPa and SLP from NCEP / NCAR reanalysis [*Kalnay et al.*, 1996]; and OLR from NOAA / NCEP [*Chelliah and Arkin*, 1992].

Figure 10. The time series of average February through May Northeast Brazil rainfall[1] anomaly index for 1849–1995 and simultaneous regressions of selected seasonal-mean fields onto this index for 1985-93. *Panel a)*: anomalies are with respect to the entire period of record. *Panel b):* COADS SLP and COADS surface vector wind superimposed upon rainfall (shading) [*Xie and Arkin, 1996]. Panel c):* COADS surface vector wind superimposed upon COADS SST. Shading and contouring conventions as in Fig. 7.

Figure A1. Longitude-time diagram of anomalies in OLR (8.75°N–11.25°S), GPI (7.5°N–10°S), SSM/I rainfall (10°N–10°S), MSU rainfall (7.5°N–10°S), and merged rainfall estimates (7.5°N–10°S). Red and blue shading for positive and negative rainfall anomalies, respectively (negative and positive OLR anomalies, respectively). Light and saturated shading for rainfall anomaly magnitudes > 2.5 and > 25.0 cm mon^{-1}, respectively (OLR anomaly magnitudes > 5 and > 30 W m^{-2}, respectively). Data sources: OLR as in Fig. 7; GPI from NOAA / NCEP; SSM/I from NASA / Goddard Space Flight Center; MSU as in Fig. 3; and the merged rainfall product from NOAA / NCEP.

Figure A2. December-January-February averages for 1986–87 minus 1988–89 in a) OLR and b) MSU rainfall. Progressively darker shading for OLR anomalies > 10, 30, 50 W m^{-2} in magnitude and rainfall anomalies > 7.5, 22.5, 37.5 cm mon^{-1} in magnitude. Solid and dashed contours indicate no change and increases in OLR (decreases in MSU rainfall) from 1986–87 to 1988–89, respectively.

---

[1] Rainfall index taken as the standardized average of standardized Fortaleza (3.7 °S, 38.5 °W) (1849-1987) and Quixeramobim (5.3 °S, 39.3°W) (1896-1987) rainfall anomalies. Values for 1988-95 obtained from Xie and Arkin *[1996].*

J. M. Wallace, T. P. Mitchell, and E. S. Sarachik, Joint Institute for the Study of Atmosphere and Ocean, Box 354235, University of Washington, Seattle, WA 98195, U.S.A.

E. M. Rasmusson, Department of Meteorology, University of Maryland, College Park, MD 20742, U.S.A.

V. E. Kousky, NOAA / NCEP Climate Prediction Center, Washington, D.C., 20233, U.S.A.

H. von Storch, Institute of Hydrophysics, GKSS, Max-Planck-Strasse 1, 21502 Geesthacht, Germany

12, in press, 1997.

Yulaeva, E., and J. M. Wallace, The signature of ENSO in global temperature and precipitation fields derived from the Microwave Sounding Unit, *J. Climate, 7*, 1719–1736, 1994.

Zebiak, S.E., Air-sea interaction in the equatorial Atlantic region, *J. Climate, 6*, 1567-1586, 1993.

Zhang, Y., J. M. Wallace, and D. S. Battisti, ENSO-like decade-to-century scale variability: 1900–93, *J. Climate*, in press, 1997.

Weare, B.C., A statistical study of the relationship between ocean temperature and the Indian monsoon., *J. Atmos. Sci., 36,* 2279-2291, 1979.

Weare, B. C., El Niño and tropical Pacific Ocean temperature, *J. Phys. Oceanogr., 12,* 17–27, 1982.

Weare, B. C., A. R. Navato, and R. E. Newell, Empirical orthogonal function analysis of Pacific sea surface temperatures, *J. Phys. Oceanogr., 6,* 671-678, 1976.

Webster, P.J., Response of the tropical atmosphere to local, steady forcing, *Mon. Wea. Rev., 100,* 518-541, 1972.

Woodruff, S. D., R. J. Slutz, R. L. Jenne, and P. M. Steurer, A comprehensive ocean-atmosphere data set, *Bull. Amer. Meteor. Soc., 68,* 1239–1250, 1987.

Woodruff, S. D., S. J. Lubker, K. Wolter, S. J. Worley, and J. D. Elms, Comprehensive Ocean-Atmosphere Data Set (COADS) Release 1a: 1980–92, *Earth Sys. Monitor, 4,* 6 pp., 1993.

Wooster, W. W., and O. Guillen, Characteristics of El Niño in 1972, *J. Mar. Res., 32,* 378–404, 1974.

Wright, P. B., J. M. Wallace, T. P. Mitchell, and C. Deser, Correlation structure of the El Niño / Southern Oscillation phenomenon, *J. Climate, 1,* 609–625, 1988.

Wyrtki, K., The annual and semiannual variation of SST in the north Pacific Ocean, *Limnol. Oceanogr., 10,* 307–313, 1965.

Wyrtki, K., El Niño – the dynamic response of the equatorial Pacific Ocean to atmospheric forcing, *J. Phys. Oceanogr., 5,* 572–584, 1975.

Wyrtki, K., The response of sea level topography to the 1976 El Niño, *J. Phys. Oceanogr., 9,* 1223–1231, 1979.

Xie, P., and P. A. Arkin, Analyses of global monthly precipitation using gauge observations, satellite estimates, and numerical model predictions, *J. Climate, 9,* 840–858, 1996.

Yukimoto, S., M. Endoh, Y. Kitamura, A. Kitoh, T. Motoi, A. Noda, and T. Tokioka, Interannual and interdecadal variabilities in the Pacific in an MRI coupled GCM, *Climate Dyn.,*

other climatologies, *J. Climate, 6,* 1301–1326, 1993.

Spencer, R. W., and J. Christy, Precise monitoring of global temperature trends from satellites, *Science, 247,* 1558–1562, 1990.

Spencer, R. W., and J. Christy, Precision and radiosonde validation of satellite gridpoint temperature anomalies, Part I: MSU channel 2, *J. Climate, 5,* 847–857, 1992.

Spencer, R. W., and J. Christy, Precision lower stratospheric monitoring with the MSU: Technique, validation, and results, 1979–91, *J. Climate, 6,* 1194–1204, 1993.

Stricherz, J., J. J. O'Brien, and D. M. Legler, Atlas of Florida State University tropical Pacific winds for TOGA 1966–1985, 250 pp., Florida State Univ., Tallahassee, 1992.

Trenberth, K. E., Spatial and temporal variations in the Southern Oscillation, *Quart. J. Royal Meteor. Soc., 102,* 639–653, 1976.

Trenberth, K. E., and T. J. Hoar, The 1990–1995 El Niño Southern Oscillation event: Longest on record, *Geophys. Res. Lett., 23,* 57–60, 1996.

Trenberth, K. E., and D. J. Shea, On the evolution of the Southern Oscillation, *Mon. Wea. Rev., 115,* 3078-3096, 1987.

van Loon, H., and R. A. Madden, The Southern Oscillation: Part I: Global associations with pressure and temperature in northern winter, *Mon. Wea. Rev., 109,* 1150–1672, 1981.

Walker, G. T., Correlation of seasonal variations in weather IX: A further study of world weather, *Mem. Indian Meteor. Dep., 24,* 275–332, 1924.

Wallace, J. M., T. P. Mitchell, and C. Deser, The influence of sea surface temperature on surface wind in the eastern equatorial Pacific: Seasonal and interannual variability, *J. Climate, 2,* 1492-1499, 1989.

Wang, B., Interdecadal changes in El Niño onset in the last four decades, *J. Climate, 8,* 267–285, 1995.

Weare, B.C., Empirical orthogonal function analysis of Atlantic surface temperatures, *Quart. J. Royal Meteor. Soc., 193,* 467-478, 1977.

Quinn, W. H., D. O. Zopf, K. S. Short, and R. W. T. Kuo Yang, Historical trends and statistics of the Southern Oscillation, El Niño and Indonesian droughts, *Fish. Bull., 76*, 663–678, 1978.

Ramage, C. S., and A. M. Hori, Meteorological aspects of El Niño, *Mon. Wea. Rev., 109*, 1827–1835, 1981.

Rasmusson, E. M., and T. H. Carpenter, Variations in the tropical sea surface temperature and surface wind fields associated with the Southern Oscillation / El Niño, *Mon. Wea. Rev., 110*, 354–384, 1982.

Rasmusson, E. M., and T. H. Carpenter, The relationship between eastern equatorial Pacific sea surface temperatures and rainfall over India and Sri Lanka, Mon. Wea. Rev., *111*, 517-528, 1983.

Rasmusson, E. M., and J. M. Wallace, Meteorological aspects of the El Niño / Southern Oscillation, *Science, 222*, 1195–1202, 1983.

Rasmusson, E. M., X. Wang, and C. F. Ropelewski, The biennial component of ENSO variability, *J. Mar. Sys., 1*, 71–96, 1990.

Reynolds, R. J., and T. M. Smith, Improved global sea surface temperature analyses using optimal interpolation, *J. Climate, 7*, 929–948, 1994.

Rowell, D.P., C. K. Folland, K. Maskell, and M. N. Ward, Variability of summer rainfall over tropical north Africa (1906-92): Observations and modelling, *Quart. J. Royal Meteor. Soc., 121*, 669-704, 1995.

Servain, J., Simple climatic indices for the tropical Atlantic Ocean and some applications, *J. Geophys. Res., 96*, 15,137-15,146, 1991.

Shukla, J., and B.M. Misra, Relationships between sea-surface temperature and wind speed over the Arabian Sea and monsoon rainfall over India, *Mon. Wea. Rev., 105*, 998-1002, 1977.

Smith, T. M., R. W. Reynolds, R. E. Livezey, and D. C. Stokes, Reconstruction of historical sea surface temperatures using empirical orthogonal functions, *J. Climate, 9*, 1403-1420, 1996.

Spencer, R. W., Global oceanic precipitation from the MSU during 1979–91 and comparisons to

theory and numerical experiments with a general circulation model, *J.Atmos. Sci., 38,* 2653-2675, 1981.

Murphy, R. C., Oceanic and climatic phenomena along the west coast of South America during 1925, *Geogr. Rev., 16,* 25–54, 1926.

Navato, A. R., R. E. Newell, J. C. Hsiung, C. B. Billing and B. Weare, Tropospheric mean temperature and its relationship to the oceans and atmospheric aerosols, *Mon. Wea. Rev., 109,* 244-254, 1981.

Nicholson, S. E., An overview of African rainfall fluctuations of the last decade, *J. Climate, 6,* 1463-1466, 1993.

Nitta, T., and S. Yamada, Recent warming of tropical sea surface temperature and its relationship to the Northern Hemisphere circulation, *J. Meteor. Soc. Japan, 67,* 375–383, 1989.

Nobre, P., and J. Shukla, Variations of sea surface temperature, wind stress, and rainfall over the tropical Atlantic and South America, *J. Climate, 9,* 2464-2479, 1996.

Palmer, T. N., Influence of the Atlantic, Pacific and Indian Oceans on Sahel rainfall, *Nature, 322,* 251-253, 1986.

Pant, G. B., and B. Parasarathy, Some aspects of an association between the Southern Oscillation and Indian summer monsoon, *Arch. Meteor, Geoph. Bioklim., B29,* 245-252, 1981.

Parker, D. E., C. K. Folland, and M. N. Ward, Sea surface temperature anomaly patterns and prediction of seasonal rainfall in the Sahel region of Africa, in *Recent Climate Change: A Regional Approach,* edited by S. Gregory, pp. 166-178, Bellhaven Press, London, 1988.

Pazan, S., and G. Meyers, Interannual fluctuations in the tropical Pacific wind field and the Southern Oscillation, *Mon. Wea. Rev., 110,* 587–600, 1982.

Philander, S. G. H., Unusual conditions in the tropical Atlantic in 1984, *Nature, 322,* 236-238, 1986.

Poulain, P. -M., Estimates of horizontal divergence and vertical velocity in the equatorial Pacific, *J. Phys. Oceanogr., 23,* 601–607, 1993.

Brazil, *Nature, 265,* 320-323, 1977.

Matsuno, T., Quasi-geostrophic motions in the equatorial area, *J. Meteor. Soc. Japan, 44*, 25-43, 1966.

McCreary, J. P., Eastern tropical ocean response to changing wind systems with application to El Niño, *J. Phys. Oceanogr., 6*, 632-645.

McPhaden, M. J., and S. P. Hayes, Variability in the eastern equatorial Pacific during 1986-1988. *J. Geophys. Res., 95*, 13,195-13,208, 1990.

McPhaden, M. J., and J. Picaut, El Niño-Southern Oscillation displacements of the western equatorial Pacific warm pool, *Science, 250*, 1385-1388, 1990.

McPhaden, M. J., A. J. Busalacchi, R. Cheney, J. -R Donguy, K. S. Gage, D. Halpern, M. Ji, P. Julian, G. Meyers, G. T. Mitchum, P. P. Niiler, J. Picaut, R. W. Reynolds, N. Smith, and K. Takeuchi, The Tropical Ocean Global Atmosphere (TOGA) Observing System: A decade of progress, *J. Geophys. Res., this issue,* 1997.

McWilliams, J. C., and P. R. Gent, A coupled air-sea model for the tropical Pacific, *J. Atmos. Sci., 35*, 962–989, 1978.

Mechoso, C. R., S. W. Lyons, and J. A. Spahr, The impact of sea surface temperature anomalies on the rainfall over northeast Brazil, *J. Climate, 3,* 812-826, 1990.

Merle, J. M. F., Variabilité thermique annuelle et interannuelle de l'ocean Atlantique équatorial Est. L'hypothése d'un <<El Niño>> Atlantique, *Oceanol. Acta, 3,* 209-220, 1980.

Merle, J. M. F., and P. Hisard, Annual cycle and interannual anomalies of sea surface temperature in the eastern equatorial Atlantic Ocean, *Deep Sea Res., 26,* 77-101, 1980.

Mitchell, T. P., and J. M. Wallace, The annual cycle in equatorial convection and sea surface temperature, *J. Climate, 5,* 1140-1156, 1992.

Mitchell, T. P., and J. M. Wallace, An observational study of ENSO variability in 1950–78 and 1979–92, *J. Climate, 9,* 3149-3161, 1996.

Moura, A. D., and J. Shukla, On the dynamics of droughts in northeast Brazil: Observations,

Julian, P. R., and R. M. Chervin, A study of the Southern Oscillation and the Walker Circulation phenomenon, *Mon. Wea. Rev., 106*, 1433–1451, 1978.

Kalnay, E., M. Kanamitsu, R. Kistler, W. Collins, D. Deaven, L. Gandin, M. Iredell, S. Saha, G. White, J. Woollen, Y. Zhu, M. Chelliah, W. Ebisuzaki, W. Higgins, J. Janowiak, K. C. Mo, C. Ropelewski, J. Wang, A. Leetmaa, R. Reynolds, R. Jenne, and D. Joseph, The NCEP / NCAR 40-year reanalysis project, *Bull. Amer. Meteor. Soc., 77*, 437–471, 1996.

Kawamura, R., A rotated EOF analysis of global sea surface temperature variability with interannual and interdecadal scale, *J. Phys. Oceanogr., 24*, 707-715, 1994.

Lamb, P. J., Large-scale tropical Atlantic surface circulation patterns associated with Subsaharan weather anomalies, *Tellus, 30*, 241-251, 1978.

Lamb, P. J., and R. A. Peppler, West Africa, in *Teleconnections Linking Worldwide Climate Anomalies*, edited by M.H. Glantz, R.W. Katz and N. Nicholls, pp. 121-189, Cambridge Univ. Press, 1991.

Lau, N. -C., and M. J. Nath, A modeling study of the relative roles of tropical and extratropical SST anomalies in the variability of the global atmosphere-ocean system, *J. Climate, 7*, 1184-1207, 1994.

Lau, N. -C., and M. J. Nath, The role of the "Atmospheric Bridge" in linking tropical Pacific ENSO events to extratropical SST anomalies, *J. Climate, 9*, 2036-2057, 1996.

Leighly, J. B., Marquesan meteorology, *Univ. Calif. Pub. Geogr., 6, No. 4*, pp. 147–172, Univ. Calif. Press, Berkeley, 1933.

Lobell, M. J., Some observations on the Peruvian coastal current, *EOS Trans. AGU*, 332–336, 1942.

Lough, J. M., Tropical Atlantic sea surface temperatures and rainfall variations in Subsaharan Africa, *Mon. Wea. Rev., 114*, 561-570, 1986.

Mantua, N. J., and N. E. Graham, Recent trends in the climate of the tropical Pacific region, submitted to *J. Climate*, 1996.

Markham, C. G., and D. R. McLain, Sea surface temperature related to rain in Ceará, Northeast

Hastenrath, S., and A. Greischar, Circulation mechanisms related to northeast Brazil rainfall anomalies, *J. Geophys. Res., 98,* 5093-5102, 1993.

Hastenrath, S., and L. Heller, On the modes of tropical circulation and climate anomalies, *Quart. J. Royal Meteor. Soc., 103,* 77-92, 1977.

Hastenrath, S., and P. Lamb, *Climatic atlas of the tropical Atlantic and eastern Pacific Ocean,* 112 pp., Univ. of Wisconsin Press, 1977a.

Hastenrath, S., and P. Lamb, Some aspects of circulation and climate over the eastern equatorial Atlantic, *Mon. Wea. Rev., 105,* 1019-1023, 1977b.

Hisard, P., Observation de réponses de type << El Niño>> dans l'Atlantique tropical oriental Golfe de Guineé, *Oceanol. Acta, 3,* 69-78, 1980.

Hoerling, M. P., A. Kumar, and M. Zhong, El Niño, La Niña, and the nonlinearity of their teleconnections, *J. Climate, in press,* 1997.

Horel, J. D., On the annual cycle of the tropical Pacific atmosphere and ocean, *Mon. Wea. Rev., 110,* 1863–1878, 1982.

Horel, J. D., V. E. Kousky, and M. T. Kagano, Atmospheric conditions in the Atlantic sector during 1983 and 1984, *Nature, 322,* 248-251, 1986.

Houghton, R. W., and Y. Tourre, Characteristics of low frequency SST fluctuations in the tropical Atlantic, *J. Climate, 5,*.765-771, 1992.

Hsiung, J., and R.E. Newell, The principal non-seasonal modes of global sea surface temperature, *J. Phys. Oceanogr., 13,* 1957-1967, 1983.

Hurlburt, H. E., J. C. Kindle, and J. J. O'Brien, A numerical simulation of the onset of El Niño, *J. Phys. Oceanogr., 6,* 621–631, 1976.

Ichiye, T., and J. Peterson, The anomalous rainfall of the 1957–58 winter in the equatorial central Pacific arid area, *J. Meteor. Soc. Japan, 41,* 172–182, 1963.

Joyce, R., and P. A. Arkin, Improved estimates of tropical and subtropical precipitation using the GOES Precipitation Index, submitted to *J. Atmos. Ocean Tech.,* 1996.

anomalies over the global tropics, *J. Climate, 5,* 371–389, 1992.

Chen, D., S. E. Zebiak, A. J. Busalacchi, and M. A. Cane, An improved procedure for El Niño forecasting, *Science, 269,* 1699–1702, 1995.

Curtis, S. and S. Hastenrath, Forcing of anomalous sea surface temperature evolution in the tropical Atlantic during Pacific warm events, *J. Geophys. Res., 100,* 15,835-15,847, 1995.

Davey, M. K., D. L. T. Anderson, and S. Lawrence, A simulation of variability in ENSO forecast skill, *J. Climate, 9,* 240–246, 1996.

Deser, C., and J. M. Wallace, El Niño events and their relation to the Southern Oscillation: 1925–1986, *J. Geophys. Res., 92,* 14,189–14,196, 1987.

Doberitz, R., Cross-spectrum analysis of rainfall and sea temperature of the equatorial Pacific Ocean, *Bonner Meteor. Abhand., 8,* 61 pp., 1968.

Eguiguren, D. V., Las nuivas de Piura, *Biol. Soc. Geogr. Lima, 4,* 241–258, 1894.

Ferraro, R. R., F. Weng, N. C. Grody, and A. Basist, An eight-year (1987-1994) time series of rainfall, clouds, water vapor, snow cover, and sea ice derived from SSM/I measurements, *Bull. Amer. Meteor. Soc., 77,* 891-905, 1996.

Folland, C. K., T. N. Palmer, and D. E. Parker, Sahel rainfall and worldwide sea temperatures, 1901-85, *Nature, 320,* 602-607, 1986.

Gadgil, S., P. V. Joseph, and N. V. Noshi, Ocean-atmosphere coupling over the monsoon regions, *Nature, 312,* 141-143, 1984.

Gill, A.E., Some simple solutions for heat-induced tropical circulation. *Quart J. Royal Meteor. Soc., 106,* 447-462, 1980.

Goddard, L., and N. E. Graham, El Niño in the 1990's, *J. Geophys. Res.,* submitted, 1997.

Graham, N.E., Decadal-scale climate variability in the 1970s and 1980s: Observations and model results, *Climate Dyn., 10,* 135–162, 1994.

Graham, N. E., and T. P. Barnett, Sea surface temperatures, surface wind divergence, and convection over the tropical oceans, *Science, 238,* 657-659, 1987.

References

Aceituno, P., On the functioning of the Southern Oscillation in the South American sector, Part I: Surface climate, *Mon. Wea. Rev., 116,* 505-524, 1988.

Barber, R. T., and F. P. Chavez, Biological consequences of El Niño, *Science, 222,* 1203–1210, 1983.

Barnett, T. P., Interaction of the monsoon and Pacific trade wind system at interannual time scales. Part I: The equatorial zone, *Mon. Wea. Rev., 111,* 756–773, 1983.

Bengtsson, L., and J. Shukla, Integration of space and in situ observations to study global climate change, *Bull. Amer. Meteor. Soc., 69,* 1130-1143, 1988.

Berlage, H. P., Fluctuations in the general atmospheric circulation of more than one year, their nature and prognostic value, *K. Ned. Meteor. Inst., Meded. Verh.*, 152 pp., 1966.

Bjerknes, J., Atmospheric teleconnections from the equatorial Pacific, *Mon. Wea. Rev., 18,* 820–829, 1969.

Bottomley, M., C. K. Folland, J. Hsiung, R. E. Newell, and D. E. Parker, *Global Ocean Surface Temperature Atlas (GOSTA),* 333 pp., Her Majesty's Stationery Office, London, 1990.

Brooks, C. E. P., and H. W. Braby, The clash of the trades in the Pacific, *Quart. J. Royal Meteor. Soc., 47,* 1–13, 1921.

Busalacchi, A., and J. J. O'Brien, Interannual variability of the equatorial Pacific in the 1960's, *J. Geophys. Res., 86,* 10,901–10,907, 1981.

Cane, M. A., Oceanographic events during El Niño, *Science, 222,* 1189–1195, 1983.

Cane, M. A., A. C. Clement, A. Kaplan, Y. Kushnir, D, Pozdnyakov, R. Seager, S. E. Zebiak, and R. Murtugudde, 20th Century Sea Surface Temperature Trends, *Science, accepted,* 1997.

Carton, J. A., and B. Huang, Warm events in the tropical Atlantic, *J. Phys. Oceanogr., 24,* 888-903, 1994.

Chelliah, M., and P. A. Arkin, Large-scale interannual variability of outgoing longwave radiation

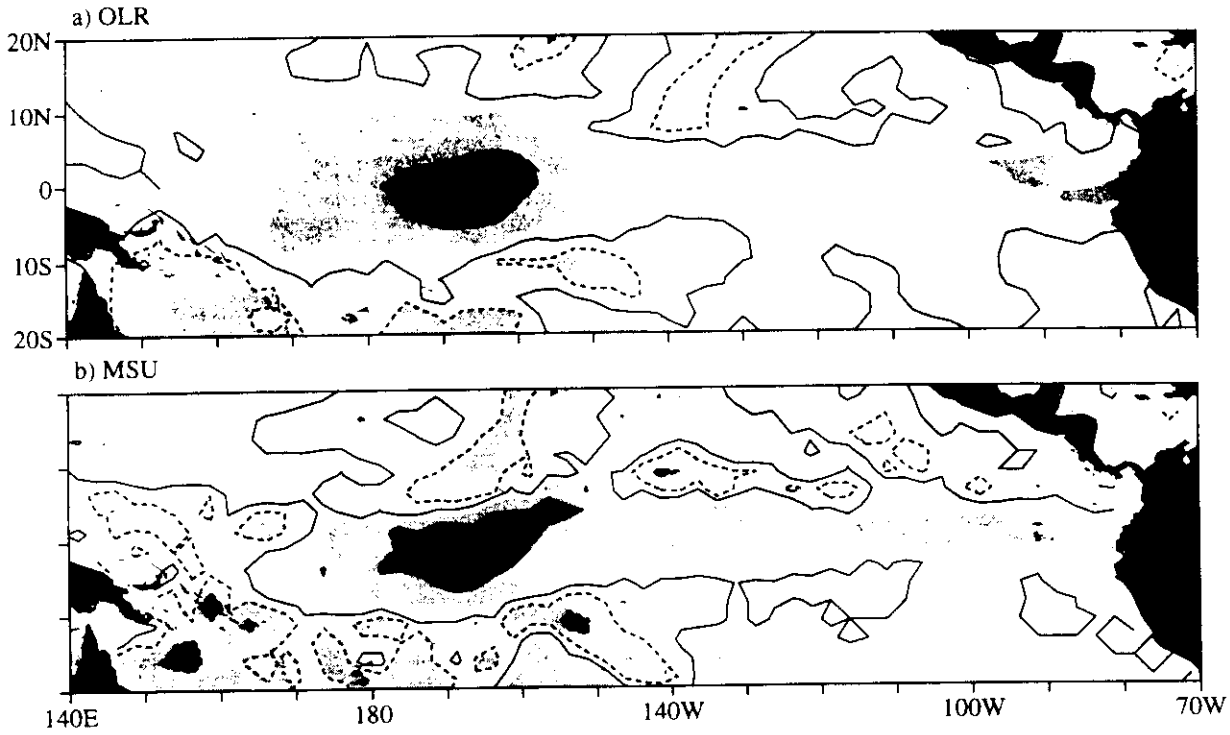

Figure A2

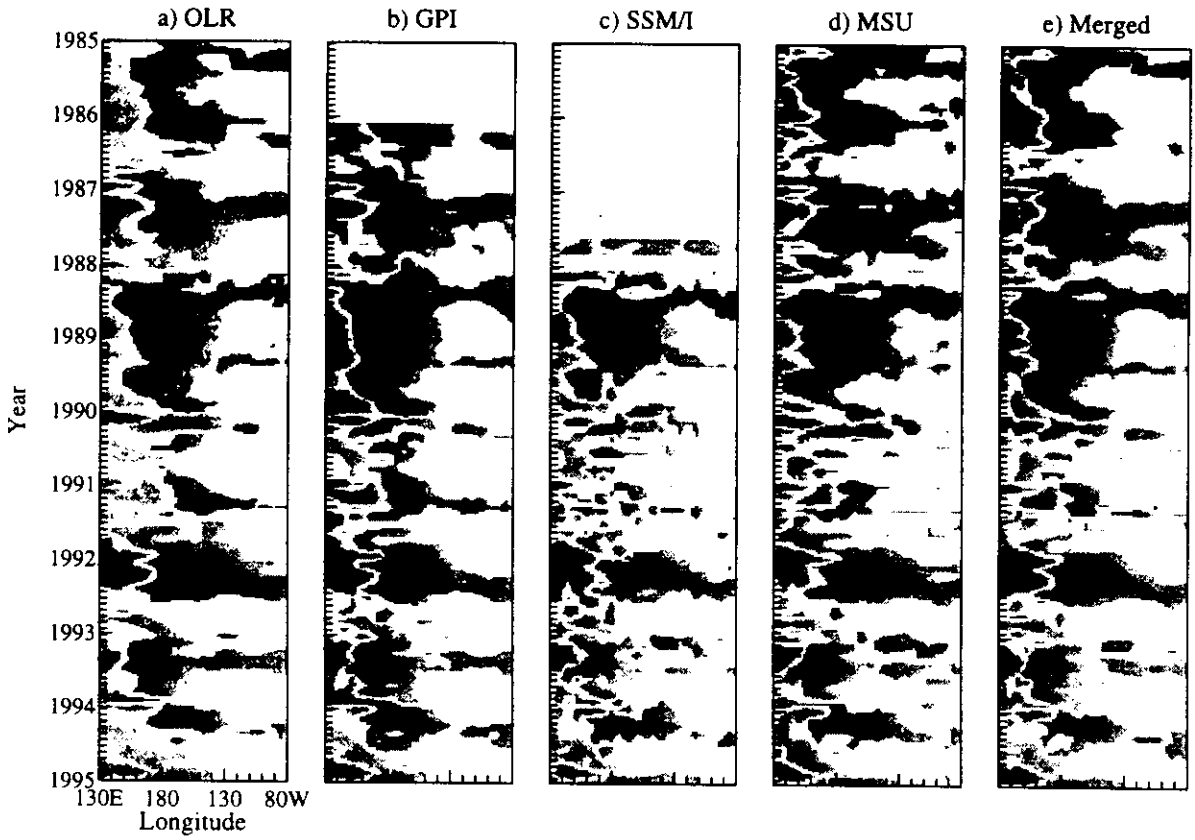
a) OLR
b) GPI
c) SSM/I
d) MSU
e) Merged
Year
1985
1986
1987
1988
1989
1990
1991
1992
1993
1994
1995
130E
180
130
80W
Longitude

Figure A1

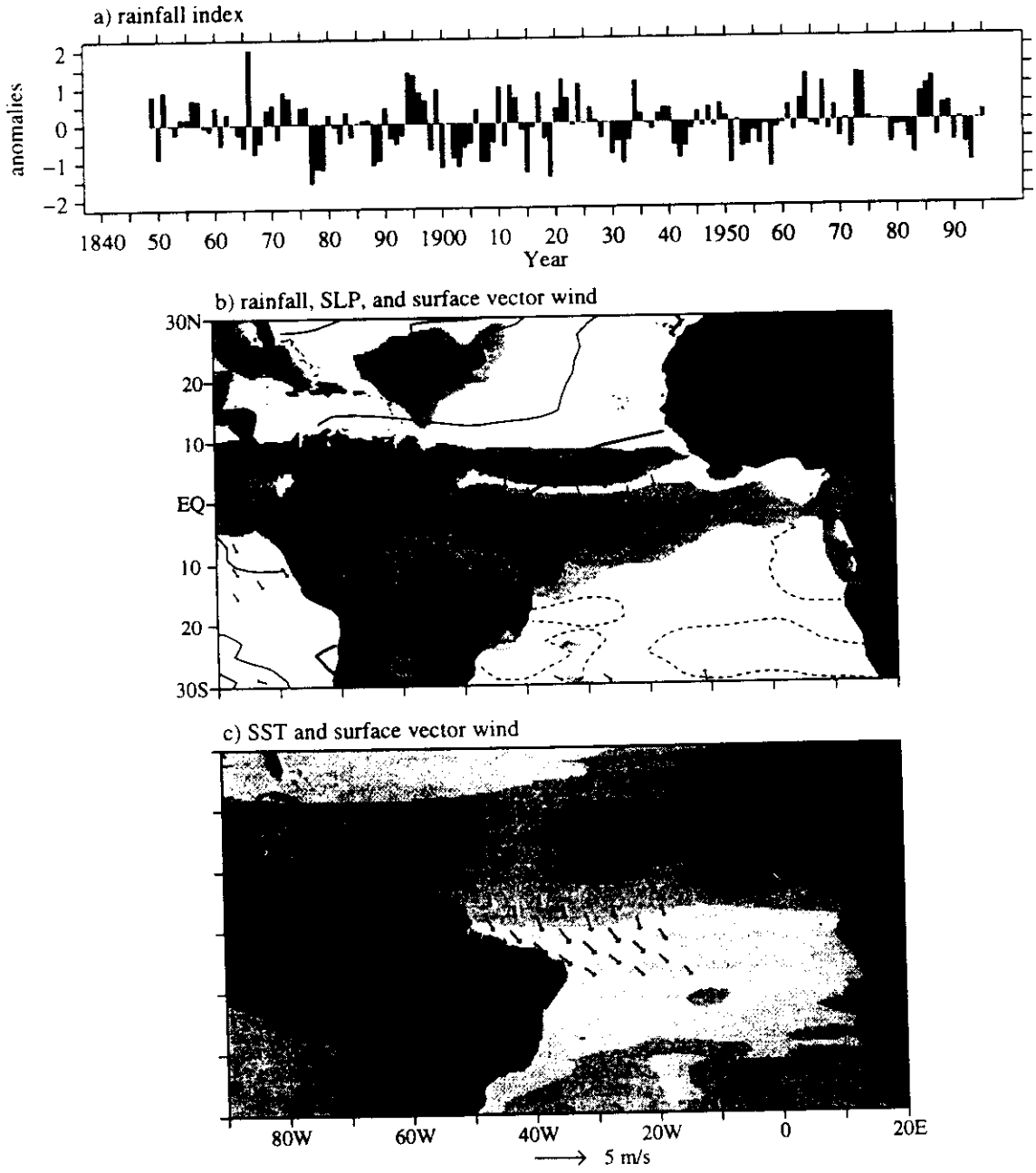
a) rainfall index
anomalies
2
1
0
−1
−2
1840 50 60 70 80 90 1900 10 20 30 40 1950 60 70 80 90
Year
b) rainfall, SLP, and surface vector wind
30N
20
10
EQ
10
20
30S
c) SST and surface vector wind
80W
60W
40W
20W
0
20E
5 m/s

Figure 10

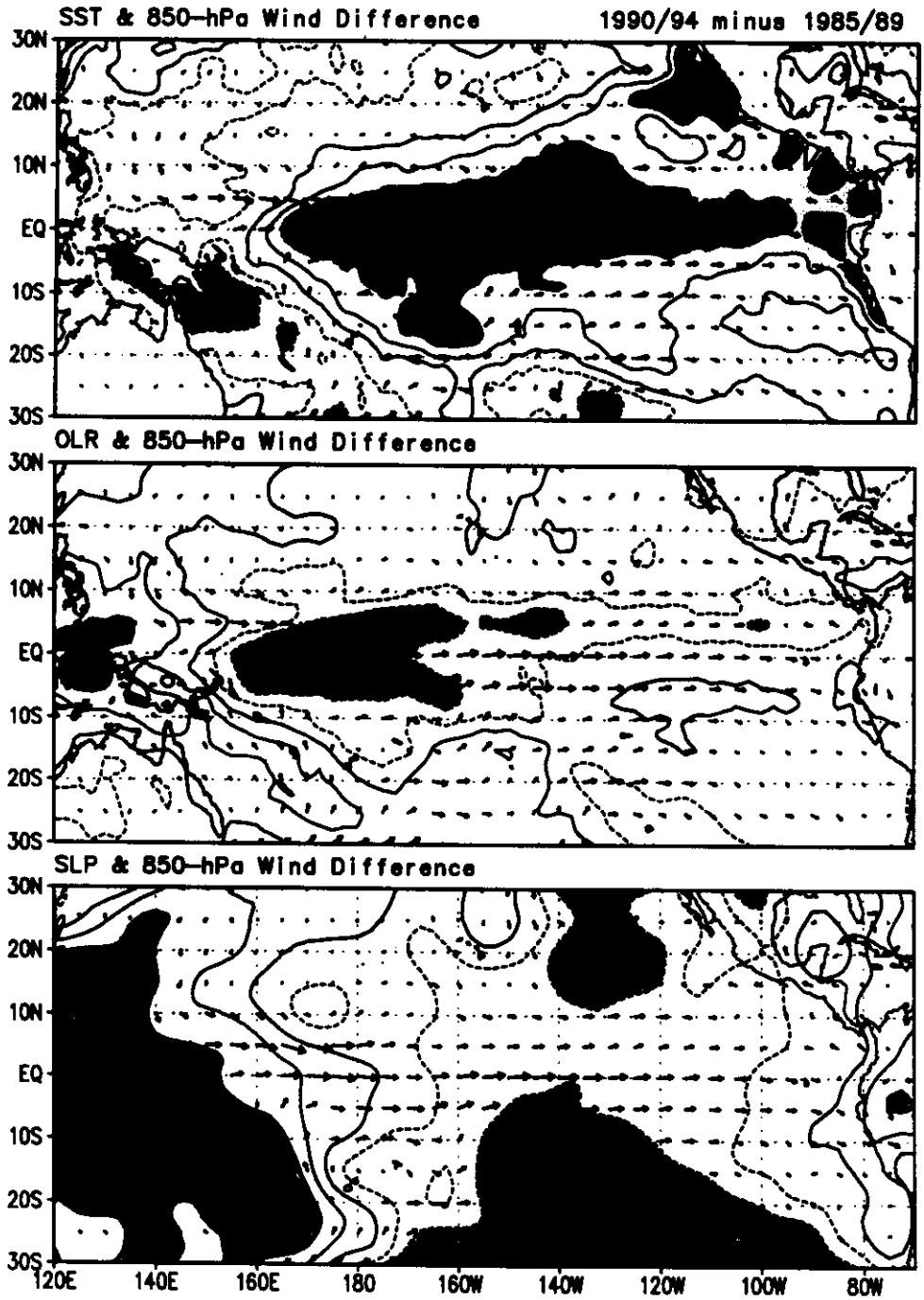
SST & 850-hPa Wind Difference
1990/94 minus 1985/89
OLR & 850-hPa Wind Difference
SLP & 850-hPa Wind Difference
30N
20N
10N
EQ
10S
20S
30S
120E
140E
160E
180
160W
140W
120W
100W
80W

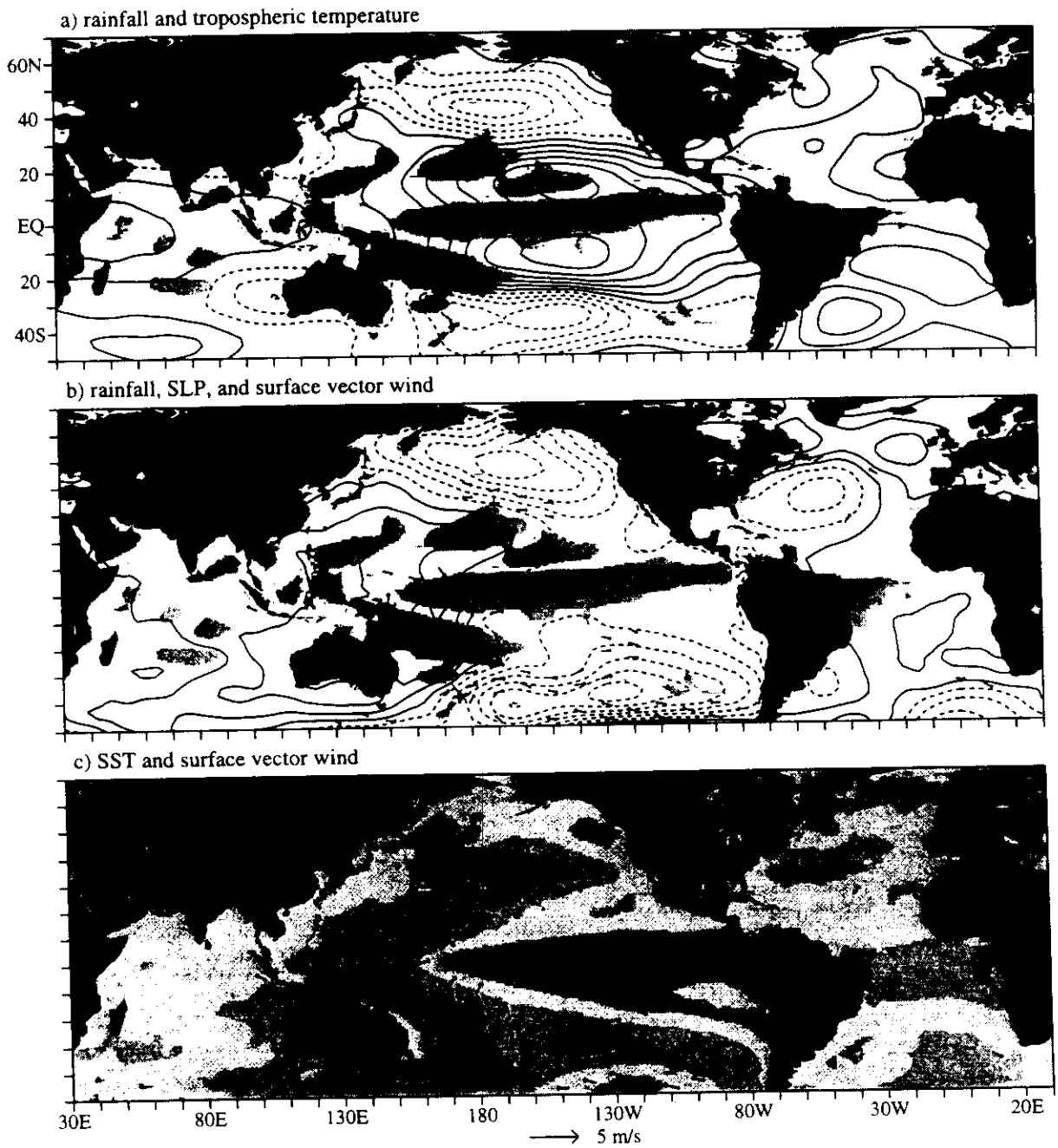
a) rainfall and tropospheric temperature
60N
40
20
EQ
20
40S
b) rainfall, SLP, and surface vector wind
c) SST and surface vector wind
30E
80E
130E
180
130W
80W
30W
20E
5 m/s

Figure 8

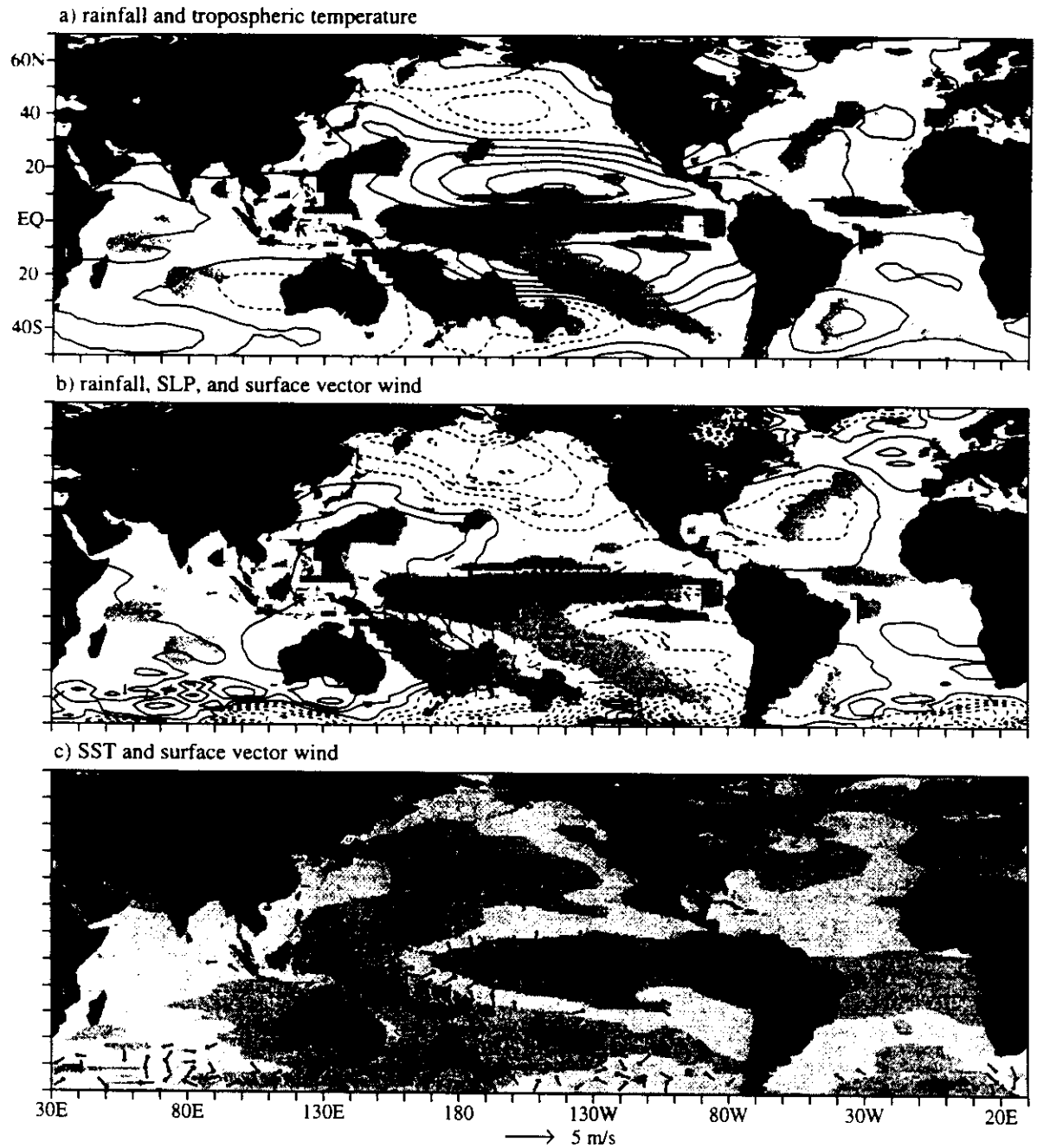
a) rainfall and tropospheric temperature
60N
40
20
EQ
20
40S
b) rainfall, SLP, and surface vector wind
c) SST and surface vector wind
30E
80E
130E
180
130W
80W
30W
20E
5 m/s

Figure 7

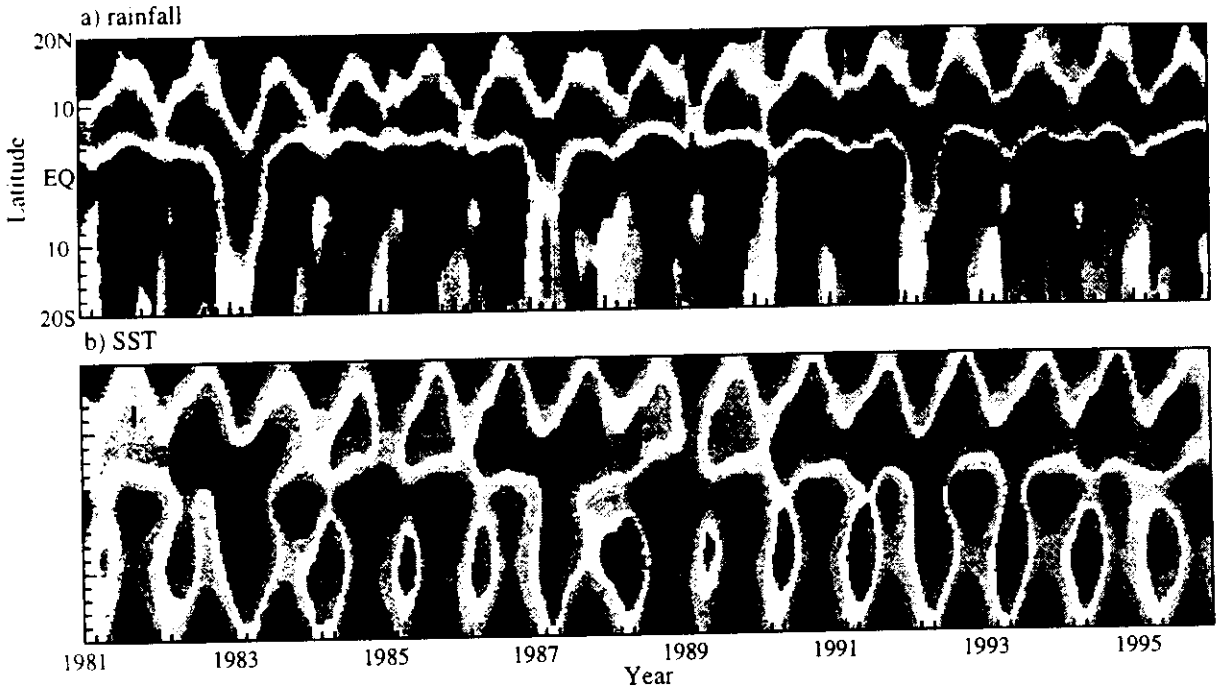
a) rainfall
20N
10
EQ
10
20S
Latitude
b) SST
1981
1983
1985
1987
1989
1991
1993
1995
Year

Figure 6

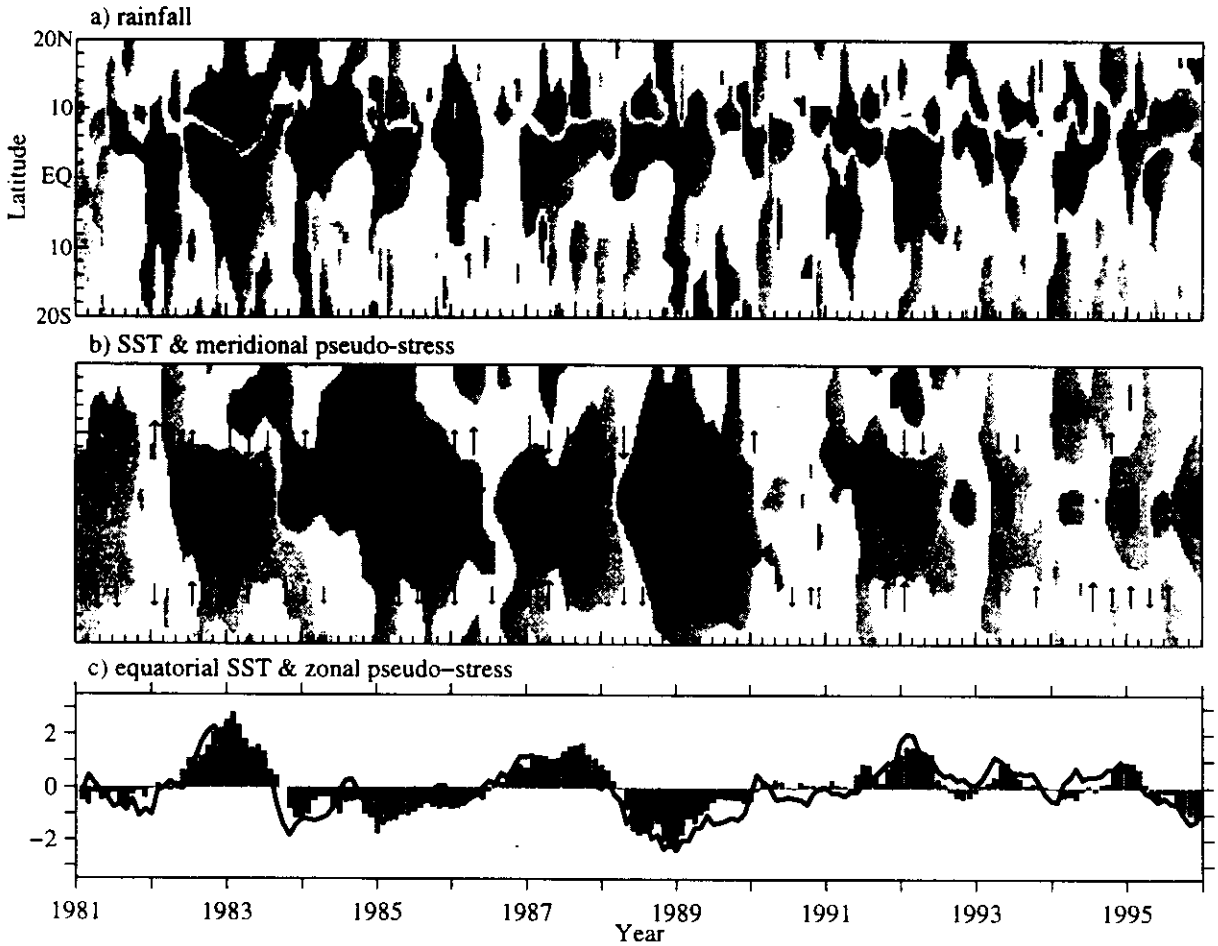
a) rainfall
20N
10
EQ
10
20S
Latitude
b) SST & meridional pseudo-stress
c) equatorial SST & zonal pseudo–stress
2
0
−2
1981
1983
1985
1987
1989
1991
1993
1995
Year

Figure 5

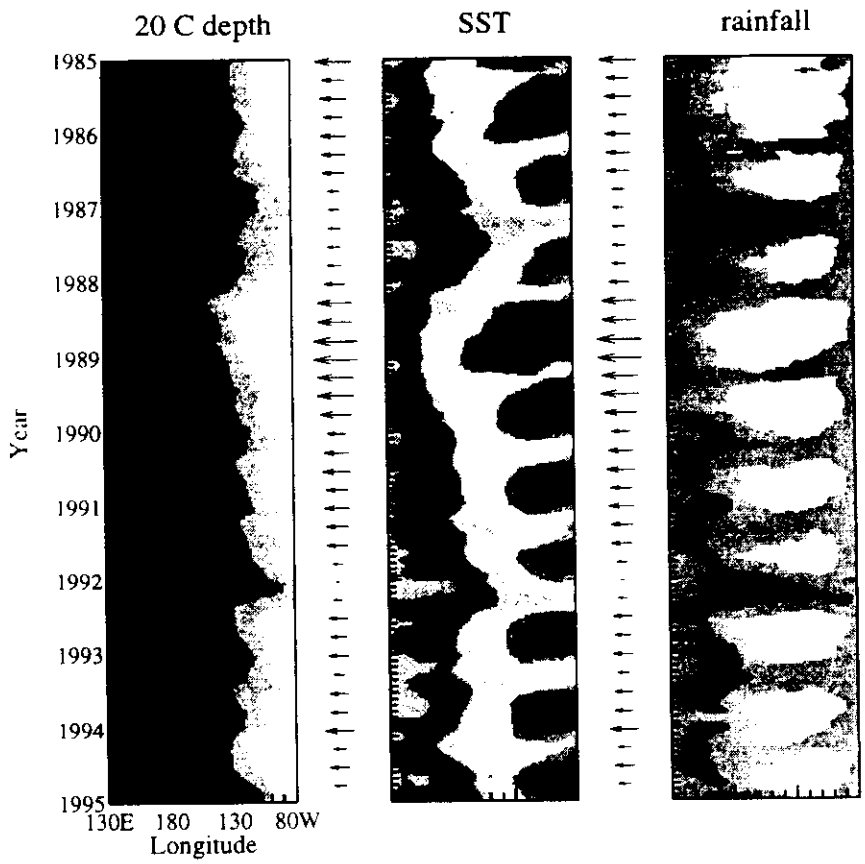
20 C depth
SST
rainfall
1985
1986
1987
1988
1989
1990
1991
1992
1993
1994
1995
Year
130E
180
130
80W
Longitude

Figure 4

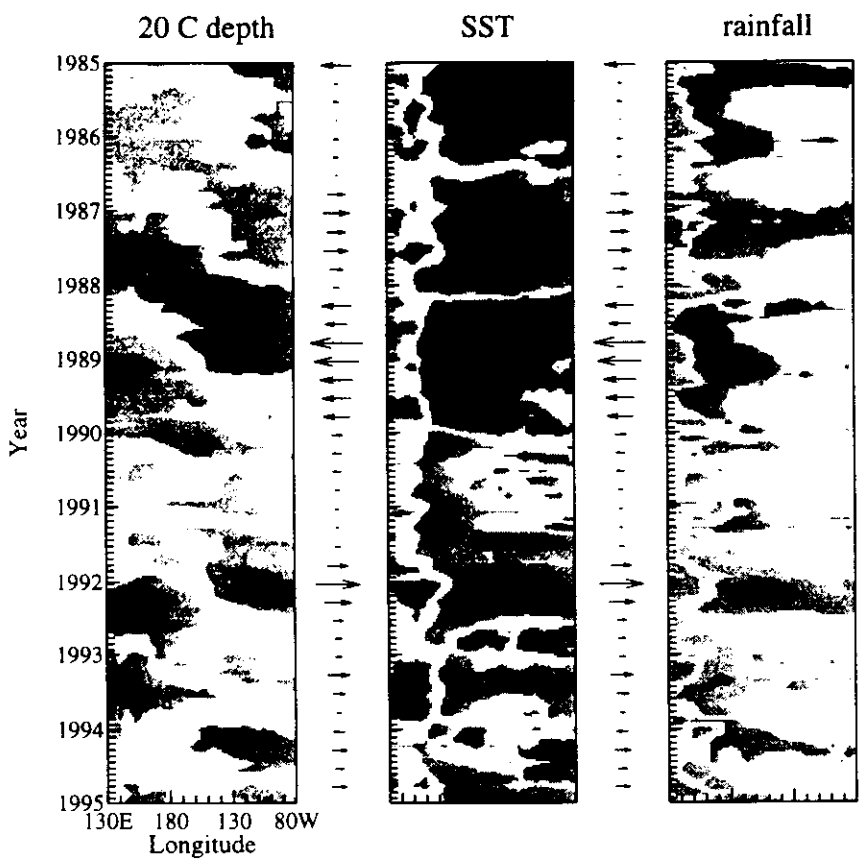
20 C depth
SST
rainfall
Year
1985
1986
1987
1988
1989
1990
1991
1992
1993
1994
1995
130E
180
130
80W
Longitude

Figure 3

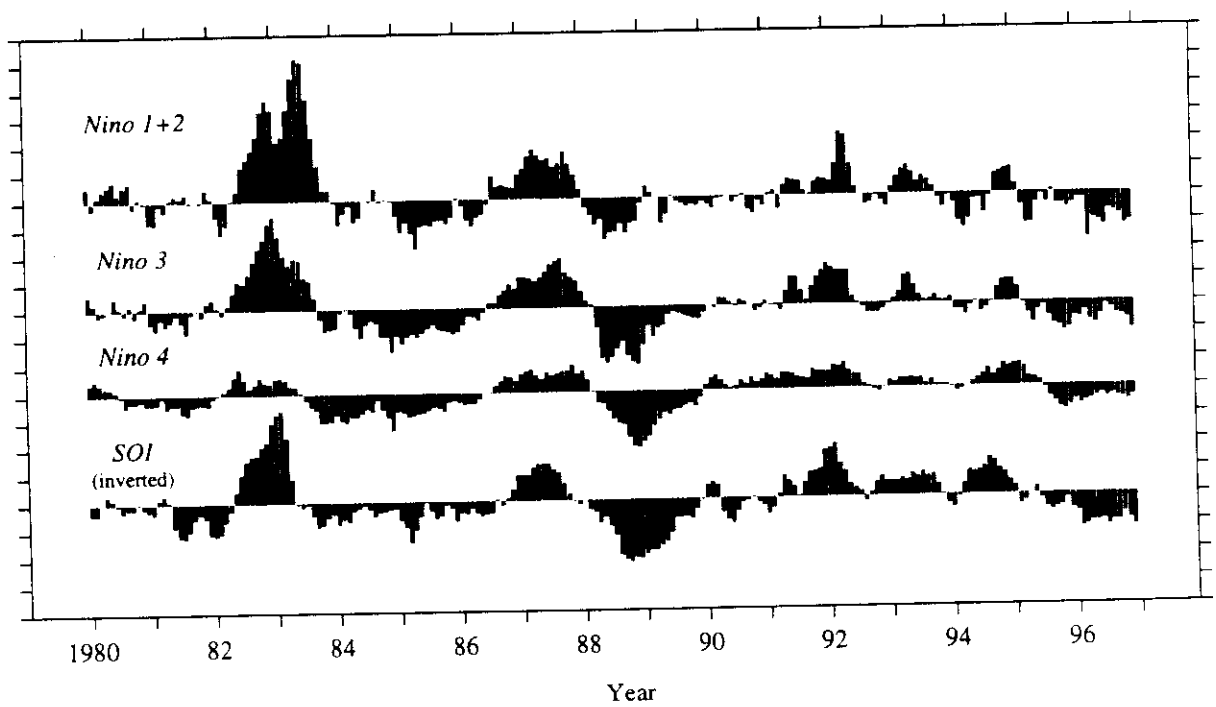
Nino 1+2
Nino 3
Nino 4
SOI
(inverted)
1980
82
84
86
88
90
92
94
96
Year

Figure 2

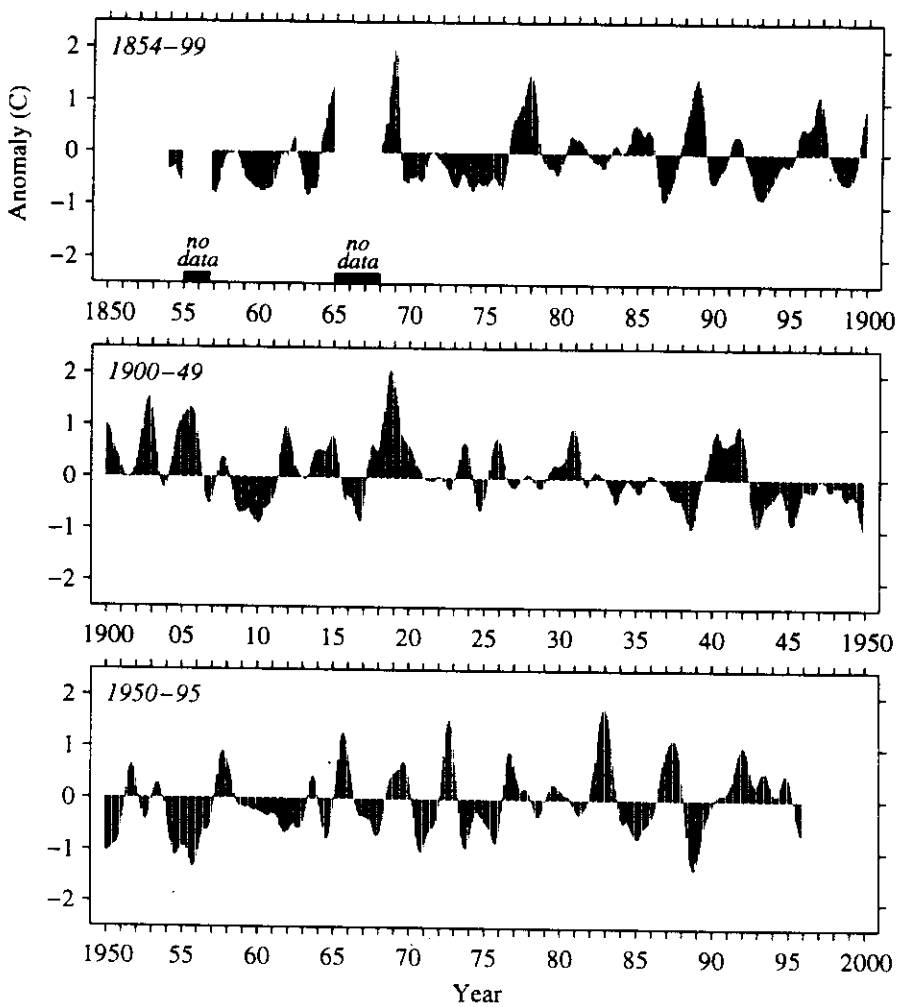
1854–99
1900–49
1950–95
no data
no data
Anomaly (C)
Year
2
1
0
−1
−2
1850
55
60
65
70
75
80
85
90
95
1900
05
10
15
20
25
30
35
40
45
1950
2000

Figure 1